

1 Editor comments

Dear authors,

I first would like to apologize for the delay in the review process. The two reviewers acknowledge the interest of the study, but they both raise questions preventing the acceptance of your manuscript without major revisions. Among the key questions raised, I think that the hypothesis of linearity dependence of organic carbon burial on astronomical forcing is far from being obvious, and impact strongly your results. This should be extensively discussed in the revised version, with adequate references. The other reviewer raised the question of existence of the $p\text{ CO}_2$ high resolution data for the Plio-Pleistocene period that should be included in your study. These two points, together with all the other questions, should be answered or discussed in the revised manuscript, that I encourage you to submit. Once the revised version received, it will go for a second round of reviews.

Best regards.

Dear editor,

We think we have addressed the concerns about our choice for linear forcing and the available $p\text{ CO}_2$ and CCD records in the revised manuscript. Below, you will find our responses to all the points by the reviewers, followed by a marked-up document with changes relative to the first version (removed words in red, added words in blue).

We look forward to receiving more feedback on the document.

Kind regards,

on behalf of all co-authors,

Ilja Kocken

2 Referee 1

General comments:

This paper explores the relationship between orbital forcing and global carbon cycles across different timescales. For this purpose, the authors simulated the response of several key components of the carbon cycles to the orbital forcing using the LOSCAR model and compared those to the composite benthic foraminiferal $\delta^{13}\text{C}$ and $\delta^{18}\text{O}$ records covering the Eocene to Miocene. They highlighted the potential dominance of 2.4 Myr eccentricity cycle in the model results and argue that this cycle maybe overshadowed by the long-term changes in the composite records.

We thank the reviewer for his/her feedback on the manuscript.

Overall, the structure of this paper is well shaped and data are clearly presented. However, I have two main concerns that need to be clarified by the authors: As suggested by the authors in the introduction of this paper, the co-occurrence of 405 and 100 kyr eccentricity maxima and relatively negative $\delta^{13}\text{C}$ and $\delta^{18}\text{O}$ values is still elusive, and different mechanisms, such as organic carbon burial linked to weathering controlled clay deposition, variations of global exogenic carbon pool, submarine methane hydrate dynamics, etc, have been suggested to address this. However, without any further discussion of these different mechanisms in the latter part of this paper, it seems to me that the authors already think the organic carbon burial plays a very important role in this co-occurrence before testing it, which doesn't make sense to me. Moreover, the authors argue that the continental shelves are very important for the organic carbon storage over astronomical time scales, which leads them to linearly force the Corg burial in marine sediment with astronomical forcing in their modelling. This doesn't make sense to me as both aspects, on the one hand, how astronomical cycles force the changes in the continental shelves, what the role of weathering has played, and why it is linear relationship between them, on the other hand, how burial of organic matter is regulated in the continental shelves, are still open questions. The authors found strong 2.4 Myr cyclicity in their model output but no signal in the composite records based on the MTM spectral analysis, which they argue the 2.4 Myr cyclicity may act purely as amplitude modulator, not as a true cycle. To me it is very important to address why 2.4 Myr cyclicity is dominant in the model output but act as an AM in the composite records as this is the key to understand the questions raised by the authors. Although the author expect to evaluate this with high-resolution proxy records in the future, I feel this part is under-discussed since this is certainly the highlight of this manuscript.

We introduce many possible mechanisms for the co-occurrence of the 405 and 100 kyr eccentricity maxima in climate records, since they are still poorly understood. We then dive into one of the possible mechanisms, using a relatively simple forcing scheme – linear forcing of organic carbon (OC) burial in the continental shelves. Since the mechanisms are largely unknown, but we do know that they must link astronomical forcing to changes in $\delta^{13}\text{C}$ and $\delta^{18}\text{O}$, we decide to force OC burial directly, and linearly, as a first approximation. OC burial is the product of sediment accumulation and organic carbon contents (corrected for porosity) and is thus linearly related to sediment accumulation, which in turn is approximately linearly related to sediment delivery to the ocean in the absence of major changes in sea level. Other factors governing OC burial (oxygen etc.) are secondary to sediment deposition. Moreover, we believe that our linear approach is preferred as a starting point, and find that it is quite capable of explaining some of the patterns we observe in climate records. We

have have added a paragraph to explain this better to the introduction.

Secondly, we have elaborated on the significance between the discrepancy between model output (2.4 Myr as a cycle) and data composite (2.4 Myr a amplitude modulation (AM)) in the model-data comparison section. Mainly, we do not expect to find AM in the model output, since there is no mechanism in the model that would introduce such forcing and there is no reason to expect it to show as an emergent property. This means that in the real world, a certain process or processes causes the 2.4 Myr cycle to be present as an AM of the shorter eccentricity cycles, that we apparently do not incorporate in this simple carbon cycle model. At this point, with the available information, it is difficult to speculate regarding the exact causes of this result although we very much agree with the reviewer that it is an important result.

I also have a few technical comments:

1. Labels for Figure 2 are missing. 2) In model-data comparison, the authors said ‘the lag of $\delta^{13}\text{C}$ to the 405 kyr eccentricity cycle is ~ 190 kyr, which is much higher than the 40 to 60 kyr during the Paleocene’, it would be better for the authors to address the phase relationship between different records using cross spectral analysis, such as ‘Application of the cross wavelet transform and wavelet coherence to geophysical time series’ by Grinsted et al., 2004. 3) For Figure 4, I recommend using the wavelet analysis to assess whether this lead-lag relationship is constant through time, see Grinsted et al., 2004 for details.
1. We have added the a–d labels.
2. Indeed, we do use cross-spectral analysis using the Blackman-Tukey (BT) method from Analyseries to calculate this 190 kyr lag in the model. Using the suggested wavelet-based analysis would allow us to estimate changes in this relationship through time. However, we have no reason to suspect that the model output will show different phases in different time-slices, since it is forced with a simple cyclic input. If we look at the model output time-series, there is also no reason to suspect temporal changes in the phasing. The estimates of 40 to 60 kyr for the lag in the data are from the literature.

We are open to applying cross-wavelet analysis, but we do not see the added value. We tried to access the Cross-Wavelet matlab script the reviewer pointed us to (from <http://www.pol.ac.uk/home/research/waveletcoherence/>) but this script was not accessible.
3. We could attempt to perform Cross-Wavelet analysis using the R-package WaveletComp (http://www.hs-stat.com/projects/WaveletComp/WaveletComp_guided_tour.pdf), but as mentioned before, we do not see the added value and are open to further editorial advice on this particular issue.

3 Referee 2

This manuscript presents an interesting modelling study of the eccentricity components in the Cenozoic carbon isotope records. Overall, the paper is well written and the obtained results are worth publishing. I nevertheless have some major comments on the model-data comparison and the overall discussion, which both appear quite incomplete and insufficient.

We thank reviewer 2 for his/her constructive and elaborate feedback on the manuscript.

Major comments

1 - The model used here computes many variables, but only a few of them are discussed. In particular, since the ocean temperatures (in the Pacific) are computed, I would expect to find a comparison between them and the ^{18}O records presented in the introduction (Figure 1). Such a comparison is not shown and not even discussed.

Our study explores the behaviour of the well-documented LOSCAR model (e.g. Zeebe 2012 GMD) under orbital forcing. The climate parametrizations in this carbon cycle model are rather simple and generate multiple output variables. In our initial submission we showed all the tracers relevant for this study. In the revised version we have added all model output in the digital supplement for completeness: it will allow the reader to evaluate alternatives. Detailing the behaviour of all tracers in the main text would not only dilute the main message, but it would also largely repeat what has been published before.

From the legend of Figure 2 (deep Pacific temperature ... are omitted from this plot because their pattern mirror that of $\{C_{\text{tot}}\}$), I understand that temperature is dominated by the carbon forcing ($p\text{ CO}_2$) and exhibits a strong 2.4 Myr oscillation. What about its amplitude? Is it compatible with data? I suspect this is not the case. The $p\text{ CO}_2$ changes are large (about a $p\text{ CO}_2$ doubling at 2.4 Myr frequency) therefore modelled temperature changes should be in the 3 to 4 °C range for rather standard values for climate sensitivity, and the corresponding ^{18}O amplitude should be in the 0.5 to 1 ‰ range. This does not seem to be compatible with data as shown on Figure 1. In any case, whatever the results, I do not understand the modelling strategy: why using a rather sophisticated model that computes many outputs, but only discussing (cherry picking?) some of them, and not others?

The model calculates temperature (TCB in the supplementary plot, we have updated the legend to “temperature”) from atmospheric CO_2 from an input temperature sensitivity parameter of 5 °C, resulting in changes of about 3 °C as estimated by the reviewer). Thus, if we simply translate these into $\delta^{18}\text{O}$, this

would result in 2.4 Myr cyclicity with a too-high amplitude ($\sim 0.75\%$) when compared to our data-composite.

However, it is important to note that the LOSCAR model is a carbon cycle model and not a climate model. Thus, its simple climate sensitivity equation relates CO_2 and temperature to each other directly, whereas in reality temperature is a function of a number of variables, including but not limited to $p\text{CO}_2$. For instance, insolation directly affects the climate system components (e.g. atmosphere, etc.), which in turn affect temperature. These insolation-driven changes to the climate system are not part of the temperature-response to CO_2 , however. This behaviour cannot be captured by the carbon cycle model. The above justifies our initial focus on $\delta^{13}\text{C}$ in the data-model comparison, rather than $\delta^{18}\text{O}$. Therefore it is not surprising that temperature, $\delta^{18}\text{O}$, and $p\text{CO}_2$ records show different power spectra, whereas our carbon cycle model output does not. Thus the lack of a strong 2.4 Myr cycle in $\delta^{18}\text{O}$ (and temperature) records does not necessarily suggest that the 2.4 Myr cycle can not be dominant in $p\text{CO}_2$.

We have added the $\delta^{18}\text{O}$ of the composite record to the analysis in the supplement, to facilitate model-data comparison (supplement fig. 6), and added a paragraph to elaborate on this to the model-data comparison section of the results and discussion.

2 – Similarly, the CCD output of the model is also not compared to the real world. This is a bit less disturbing, since the authors are not showing any CCD reconstructions over this time span. But such data exist, though probably with low resolution. For instance, according to Päelike et al (Nature, 2012), the Pacific CCD is deep and stable during this time (Oligocene-Miocene) up to about 18.5 Ma. Again, this does not seem consistent with the model results. Interestingly, they also observe rather large changes in the CCD during the Eocene (CAE events), that may, or may not, correspond to the simulated changes in this paper? In any case, some thorough discussion of the CCD outputs with respect to observations seems to me absolutely necessary. Again, what is the point of computing these variables, if not for performing some comparison with data?

Comparing the CCD model output changes to those reconstructed by Päelike et al. (2012) would be a nice addition to the manuscript. In terms of absolute values this exercise would not be very informative, however, since it is dependent on multiple input parameters of the model. The main aim of this study is not necessarily to get the best agreement between model predictions and data based reconstructions, but rather to study the possible underlying mechanisms.

We have included a section on this in the model-data comparison section. While we were able to perform some analysis with moderate success, as described in the revised manuscript, problems arise due to problems with the age-models for the Eocene. Resolving these problems for all individual records is beyond the scope of this manuscript.

3 – According to the final sentence, high resolution $p\text{CO}_2$ proxies would be necessary to check if a strong 2.4 Myr signal is present or not over the Cenozoic, as suggested by the model. As mentioned in my first comment, such a strong eccentricity signal in greenhouse gases should probably have already been detected in the (climate) ^{18}O data. But more importantly, such $p\text{CO}_2$ proxy data are in fact readily available for the Plio-Pleistocene (eg. Bartoli et al., 2011; Seki et al, 2010; ...) and no such large ($2\times$) $p\text{CO}_2$ changes are seen, while large climatic changes are obvious. A simple model also based on organic carbon burial on continental margins was proposed recently (Paillard, CP, 2017) to account both for the ^{13}C and the $p\text{CO}_2$ data over this period.

The $p\text{CO}_2$ records that the referee refers to (e.g. Bartoli et al. 2012, Seki et al. 2010) have neither the length nor the resolution to pin down a possible 2.4 Myr cycle, but we have added a short paragraph on them to the discussion. New, long $p\text{CO}_2$ proxy records are required to establish a possible 2.4 Myr cyclicity.

We have commented on the likeliness of the $\delta^{18}\text{O}$ record being reflective of CO_2 dynamics in the discussion. We thank the referee for bringing the very relevant Paillard (2017) paper to our attention. It is a relevant reference for our study and we have acknowledged and addressed it as such in the revised manuscript.

4 – Spectral analysis represents a rather large part of the paper (Figs 3 to 6). Still, I do not quite understand how this helps for the discussion or for the conclusions, beyond the (quite expected) fact that long-term processes are acting as low-pass filters. Either I missed some important point, or probably there is a far too large weigh on spectral analysis in this paper.

Spectral analysis indeed forms the backbone of this paper, as it is the primary tool by which we assess the presence and impact of the 2.4 Myr and 405 kyr cycles. We deliberately included detailed spectral analysis based on multiple techniques, to inform the reader about, *inter alia* the spectra of different model (and data) variables, amplitude modulation thereof and cross-correlation between variables.

5 – The same comment applies for the use of red noise in the experiments. Obviously, there is here some (rather implicit) attempt to fit the spectrum of the data with a deterministic model plus a red noise. But what is the point? I understand that red noise fitting is useful for spectral line detection. But this is not the topic of the paper. What do the noisy experiments tell us about the dynamics of organic carbon on continental margins? Does a nice spectral fit help the authors to make their point? I am personally not convinced.

In our simulations we use white noise as input which results in red-noise in model output. The goal of adding relatively strong white noise to the astronomical forcing (50/50 noise/signal), is to assess how our simulated signal could be perturbed by unknown/stochastic processes. We agree that creating a nice spectral fit to the data is of a secondary/non-pertinent nature and not the main focus of our study. We have modified the material and methods section to articulate this.

Other comments

6 – Page 4 line 18; Page 10 line 3 and line 10 shifting of spectral power. I certainly do not recommend using this word shifting in the current context. In signal processing, a spectral shift is a change of frequency between input and output. This is not the case here, since output frequencies are exactly the same as input ones. The authors are referring possibly to the fact that high frequencies are damped. This is simply called a low-pass filter, not a frequency shift. Or possibly that the amplitude modulation of the forcing can be extracted thanks to some non-linearity of the model (or “clipping” of the forcing). But again, this is not a “shift” in frequency, but a de-modulation (ie. the most simple tone-combination).

We thank the referee for clarification. We have rephrased ‘shifting of spectral power’ to low-pass filtering throughout the manuscript.

7 – Page 7, line 7 : ETP could be considered more objective . I do not understand why. From a mathematical viewpoint, using an insolation forcing is a parametric choice (eg. choosing latitude and season). ETP is also parametric (relative weigh of tilt and precession). Furthermore, in ETP, the phasing of precession is arbitrarily fixed to 2 values only (a plus or a minus sign), while choosing a specific season offers more freedom. Insolation is more physically based, ETP is not. Obviously, there is no specific reason to choose 65°N in summer, since there are no ice sheet present at this location. In the context of the model presented here, a much more simple and objective choice would be to use only one parameter: eccentricity, or tilt, or precession only. Then the discussion on mechanisms would be easier. Since the focus is on the 405 kyr and 2.4 Myr eccentricity frequencies in the carbon system, I am not sure that using tilt in the forcing is relevant (except may be to discuss the 1.2 Myr modulation vs the 2.4 Myr eccentricity one, but this is probably not quite the topic).

We agree, we have adjusted our wording in these lines and included separate model runs for eccentricity and precession to the supplement (suppl. fig. 9) and have included discussion of these in the main text discussion. For completeness, runs with 65°N and 30°N insolation curves as forcing were also added to the supplement (suppl. fig. 9).

8 – Legend of Figure 2: atmospheric $p\text{CO}_2$ is shown on the figure, though the legend says just the opposite.

We have revised the legend.

9 – Page 10 line 17: $180^\circ \dots$ out-of-phase. No, since out-of-phase means that there is no phase relationship. Here, it is in anti-phase, something very similar to in-phase.

We have revised out-of-phase to in anti-phase.

10 – Page 11 line 9: $\delta^{13}\text{C}$ minima are phased with ETP maxima. No. The authors probably mean that $\delta^{13}\text{C}$ minima are compared with ETP maxima, or equivalently that the relationship between $\delta^{13}\text{C}$ and ETP is measured by the phasing between $\delta^{13}\text{C}$ and ETP.

We have revised the wording to more clearly reflect our approach.

11 – Page 11 line 26 : 0.5 Myr please add exponent -1.

Exponent -1 was added.

12 – Many figure legends in the supplement are incomplete or inconsistent with the figure. which makes it difficult to understand. . . Figure 1: 3 colored curves but only 2 description. Figure 2: A/The red and purple curves are CO_2 and pacific temperature, but which one is which? According to B, purple might be CO_2 , but what is “tcb”? Figure 3: What is the green curve? Figure 6: The legend mentions ^{18}O records, but the figures displays apparently only ^{13}C one.

Figure 1: These are actually not three colours, but two lines with low opacity. We have chosen different colours to improve readability of the figure.

Figure 2: red = temperature, purple = CO_2 . We have changed the legend in (b).

Figure 3: The purple curve is the data composite $\delta^{13}\text{C}$, while the green curve is $\delta^{13}\text{C}$ model output for the specified run. The colours have been changed and the legend has been updated.

Figure 6: We have re-added the $\delta^{18}\text{O}$ records to the figure.

References:

Pälike H et al. A Cenozoic record of the equatorial Pacific carbonate compensation depth. *Nature* (2012) vol. 488 (7413) pp. 609-614.
Bartoli G et al. Atmospheric CO_2 decline during the Pliocene intensification of Northern Hemisphere glaciations. *Paleoceanography* (2011) vol. 26 (4).
Seki et al. Alkenone and boron-based Pliocene $p\text{CO}_2$ records. *Earth Planet. Sci. Lett.* (2010) vol. 292 (1-2) pp. 201-211.
Paillard D. The Plio-Pleistocene climatic evolution as a consequence of orbital forcing on the carbon cycle. *Cli*

The 405 kyr and 2.4 Myr eccentricity components in Cenozoic carbon isotope records

Ilja J. Kocken¹, Margot J. Cramwinckel¹, Richard E. Zeebe², Jack J. Middelburg¹, and Appy Sluijs¹

¹Department of Earth Sciences, Faculty of Geosciences, Utrecht University, Princetonlaan 8a, 3584 CB, Utrecht, The Netherlands

²Department of Oceanography, University of Hawai'i at Mānoa, 1000 Pope Road, HI 96822, Honolulu, USA

Correspondence: Ilja J. Kocken (i.j.kocken@uu.nl)

Abstract. Cenozoic stable carbon ($\delta^{13}\text{C}$) and oxygen ($\delta^{18}\text{O}$) isotope ratios of deep-sea foraminiferal calcite co-vary with the 405 kyr eccentricity cycle, suggesting a link between orbital forcing, the climate system, and the carbon cycle. Variations in $\delta^{18}\text{O}$ are partly forced by ice-volume changes that have mostly occurred since the Oligocene. The cyclic $\delta^{13}\text{C}$ – $\delta^{18}\text{O}$ ~~eo-variations-are~~ co-variation is found in both ice-free and glaciated climate states, however. Consequently, there should be a mechanism that forces the $\delta^{13}\text{C}$ cycles independently of ice-dynamics. In search of this mechanism, we simulate the response of several key components of the carbon cycle to orbital forcing in the Long-term Ocean-atmosphere-Sediment Carbon cycle Reservoir model (LOSCAR). We force the model by changing the burial of organic carbon in the ocean with various astronomical solutions and noise, and study the response of the main carbon cycle tracers. Consistent with previous work, the simulations reveal that low frequency oscillations in the forcing are preferentially amplified relative to higher frequencies. However, while oceanic $\delta^{13}\text{C}$ mainly varies with a 405 kyr period in the model, the dynamics of dissolved inorganic carbon in the oceans and of atmospheric CO_2 are dominated by the 2.4 Myr cycle of eccentricity. This implies that the total ocean and atmosphere carbon inventory is strongly influenced by carbon cycle variability that exceeds the time scale of the 405 kyr period (such as silicate weathering). To test the applicability of the model results, we assemble a long (~ 22 Myr) $\delta^{13}\text{C}$ and $\delta^{18}\text{O}$ composite record spanning the Eocene to Miocene (34 to 12 Ma) and perform spectral analysis to assess the presence of the 2.4 Myr cycle. We find that, while the 2.4 Myr cycle appears to be overshadowed by long-term changes in the composite record, it is present as an amplitude modulator of the 405 and 100 kyr eccentricity cycles.

Copyright statement. Ilja J. Kocken, 2018

1 Introduction

During the Cenozoic (past ~~66 Ma~~ 66 Myr) the Earth's climate system gradually shifted from an ice-free greenhouse world to an ice-house world with massive ice sheets at both ~~hemispheres~~ poles (Zachos et al., 2001). Orbital forcing – quasi-cyclic changes in the climate system as a result of changes in the orbital configuration of the Earth (Milankovitch cyclicity) – caused superimposed variability in the climate-system drivers and carbon cycle on 10^4 to 10^5 year time scales. This has been shown

in numerous palaeoclimate proxy records, notably stable carbon isotope ($\delta^{13}\text{C}$) and oxygen isotope ($\delta^{18}\text{O}$) ratios of deep-sea foraminifera. Particularly distinctive is the imprint of the 405 kyr eccentricity term (Westerhold et al., 2011) on climate and the carbon cycle, under both ice-free (Paleocene–Eocene, Westerhold et al. 2011; Laetano et al. 2015) and glaciated (Oligocene–Miocene, Pälike et al. 2006; Holbourn et al. 2015) climate regimes within the Cenozoic (Fig. 1). On this timescale, $\delta^{13}\text{C}$ co-varies in phase with $\delta^{18}\text{O}$, although the latter also responds strongly to the short eccentricity cycles (95 and 126 kyr). Similar to the shorter eccentricity cycles, the 405 kyr eccentricity cycle has a minor effect on total annual insolation (Laskar et al., 2004), but dominantly acts on the climate system as an amplitude modulator of precession, causing a greater seasonal contrast during eccentricity maxima. Changes in foraminiferal $\delta^{18}\text{O}$ primarily represent changes in global ice volume and deep-sea temperatures. Changes in $\delta^{13}\text{C}$ represent ocean-wide changes in the partitioning of carbon pools with different isotopic signatures among ocean, atmosphere, and rock reservoirs. The co-variance of oxygen and carbon isotopes therefore implies a coupling of climate and the carbon cycle, where $\delta^{13}\text{C}$ and $\delta^{18}\text{O}$ minima correspond with eccentricity maxima, or periods of increased seasonal contrast. It is important to note, however, that orbital-scale variability is a function of both cyclic forcing and other, probably non-cyclic variability on different time-scales ~~from (e.g. climate noise, tectonics, etc.~~ from tectonics).

On time scales $>10^6$ yr, the $\delta^{13}\text{C}$ of the global exogenic carbon pool is largely controlled by carbon burial on the continental margins, where the isotopic composition of the buried carbon is mainly determined by the ratio between inorganic carbon and organic carbon (C_{org}) (Berner et al., 1983). Increases in ^{13}C -depleted C_{org} burial are caused by increased delivery of clays through river runoff, as C_{org} is primarily buried in association with clay particles (Hedges and Keil, 1995). One might suspect that clay supply and burial increase during periods of increased seasonal contrast (eccentricity maxima), because this would ~~both~~ optimize weathering, erosion, and transport. In this scenario, the resulting enhanced C_{org} burial would lead to $\delta^{13}\text{C}$ maxima in the water column. However, we observe the opposite phase relation between eccentricity and $\delta^{13}\text{C}$ in palaeorecords. Alternatively, clay formation may be optimized during phases of year-round relatively wet conditions in soils to facilitate ~~plagioclase silicate~~ weathering and clay formation. If the system is not limited by transport rates, this scenario is more likely to occur during periods of low seasonal contrast (eccentricity minima), resulting in the observed phase relation between eccentricity and $\delta^{13}\text{C}$.

Various other forms of organic carbon sequestration may be the cause of the recorded phasing. For example, increased burial of C_{org} may occur on land during eccentricity minima because constant precipitation above peat lands provides conditions for development of year-round soil anoxia (Kurtz et al., 2003; Zachos et al., 2010). The resulting ^{13}C -enriched global exogenic carbon pool would be consistent with the phase relation we see in sediment records. This mechanism may be problematic, however, because it does not explain the consistent patterns throughout the Cenozoic, as terrestrial basins were unlikely stable over tens of millions of years. Another factor that might influence ~~both~~ the total mass and isotopic composition of inorganic carbon in the oceans ~~consists of~~ involves submarine methane hydrate dynamics. Microbes in continental margin sediments produce biogenic methane from C_{org} . This methane, which has $\delta^{13}\text{C}$ values of ~~up~~ down to -70‰ VPDB, can be temporarily stored in methane hydrates (Dickens, 2003, 2011). The total mass of methane stored in hydrates is affected by deep sea temperature and could thus be controlled by orbital cycles. Assuming a ~~constant~~ steady sediment methane production, more biogenic methane is ~~dereetly~~ directly mixed into the exogenic carbon pool under relatively warm climates (Dean et al., 2018).

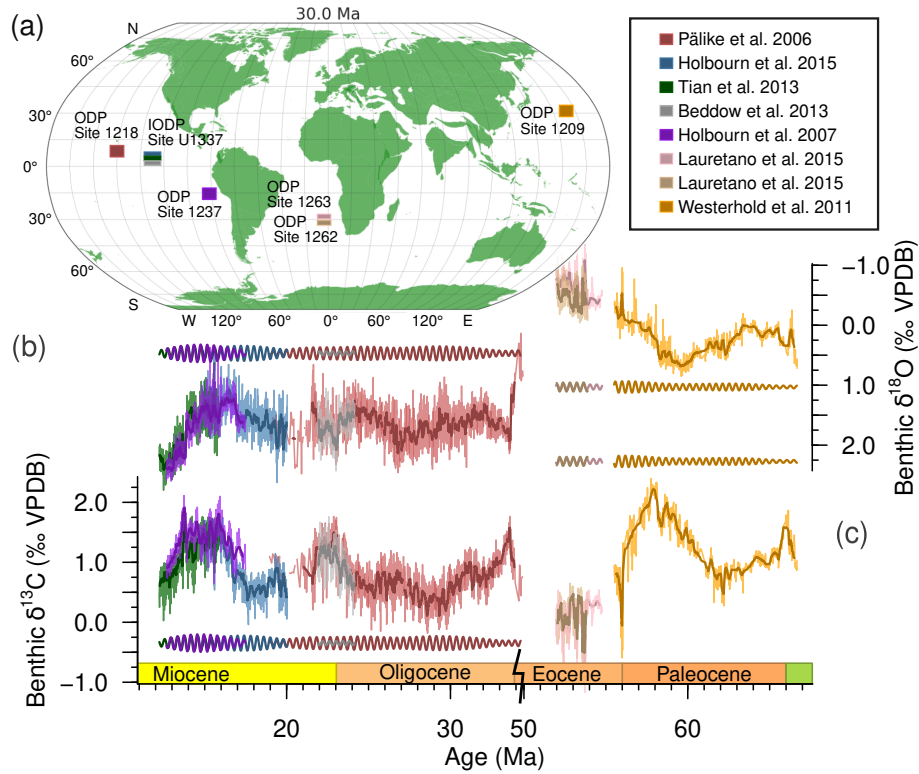


Figure 1. Long-term high resolution benthic foraminiferal stable carbon and oxygen isotope records show 405 kyr cyclicality. (a) Palaeoceanographic reconstruction of 30 Ma with approximate site locations. Map generated with GPlates, using the rotation frame and tectonic reconstruction of (Matthews et al., 2016). Data from references in the legend show the 405 kyr periodicity in the $\delta^{18}\text{O}$ (b) and $\delta^{13}\text{C}$ (c) records throughout the Cenozoic at various sites in the Pacific. Darker lines going through the records represent 20-point moving averages while darker lines at arbitrary heights represent the 405 kyr filtered records (at $2.47 \pm 0.15 \text{ Myr}^{-1}$). The Westerhold et al. (2011) record was converted to the GTS2012 (Gradstein et al., 2012) time scale by converting magnetic chron ages and placing the PETM onset at 56.0 Ma. Note the ~16 Myr x-axis break in the Eocene.

Under colder climates, more methane is trapped in hydrates, resulting in an exogenic carbon pool that is relatively ^{13}C -enriched relative to the warm phase. This would also result in the co-occurrence of 405 and 100 kyr eccentricity maxima and relatively negative $\delta^{13}\text{C}$ and $\delta^{18}\text{O}$ values. ~~In~~ However, in Paleocene–Eocene sediment records, methane hydrate dynamics cannot explain the co-occurrence and cyclicality of $\delta^{13}\text{C}$ and $\delta^{18}\text{O}$, because they would result in a slope of $\Delta\delta^{13}\text{C} - \Delta\delta^{18}\text{O}$ that is very different from the one observed (Zeebe et al., 2017). They may play a role in the Oligocene and Miocene, ~~however~~ (Pälke et al., 2006; Holbourn et al., 2015; Tian et al., 2013), but could also be related to changes in ice-volume (see below). Given the intermediate ~~ocean-depth-ocean-depth~~ temperature response to orbital variability and seasonal contrast in a fully coupled climate model (Lunt et al., 2011), methane hydrate dynamics could be a plausible explanation for coupled $\delta^{13}\text{C}$ and $\delta^{18}\text{O}$ variability.

Table 1. Possible mechanisms that can cause $\delta^{13}\text{C}$ – $\delta^{18}\text{O}$ to co-occur, as a result of input eccentricity ϵ forcing maxima (\uparrow) and minima (\downarrow).

Mechanism	ϵ	Response	Caveat/Prerequisite
Clay transport	\uparrow	\uparrow weathering $\implies \uparrow$ clay transport $\implies \uparrow C_{\text{org}}$ burial $\implies \uparrow \delta^{13}\text{C}$	Does not match data
Clay production	\downarrow	\uparrow clay formation $\implies \uparrow C_{\text{org}}$ burial $\implies \uparrow \delta^{13}\text{C}$	Weathering is not limiting
Peat-land soil storage	\downarrow	year-round anoxia $\implies \uparrow C_{\text{org}}$ sequestration in peat-land soils $\implies \uparrow$ remaining exogenic $\delta^{13}\text{C}$	Land-reservoir stable over millions of years
Methane hydrate reservoir	\uparrow	\uparrow seasonal contrast $\implies \uparrow$ intermediate water temperature \implies methane hydrate dissolution $\implies \downarrow \delta^{13}\text{C}$	Not in Paleocene–Eocene
Ice-sheet dynamics	\uparrow	\uparrow surface-air temperatures $\implies \downarrow$ in ice-volume sub-shelf melt, associated with $\downarrow \delta^{13}\text{C}$	Requires presence of ice-sheets

Alternatively, ice-sheet dynamics have been proposed as the origin of the 405 kyr cycle for the past 35 Ma (de Boer et al., 2014). In a 3D ice sheet and climate model, increased insolation with higher surface-air temperature triggers a reduction in ice volume through sub-shelf melting, which can be linked to a decrease in $\delta^{13}\text{C}$ -values through changes in the carbon cycle (de Boer et al., 2014). While the 405 kyr cycle [in stable isotopes](#) can be simulated adequately for the past 5 Myr (de Boer et al., 2014), astronomical pacing of the carbon cycle in the early Paleogene – with the absence of permanent ice-sheets – means that this mechanism alone does not explain the link between the carbon cycle, astronomical forcing, and climate variability throughout the Cenozoic.

It is unknown which mechanism is responsible for the co-occurrence of the 405 and 100 kyr eccentricity cycles in climate records, but we do know that they must link astronomical forcing to changes in $\delta^{13}\text{C}$ and $\delta^{18}\text{O}$. We decide to explore C_{org} burial in the oceans. In nature, continental margins provide the largest C_{org} storage potential over astronomical time scales (Berner, 1982). C_{org} burial is the product of sediment accumulation and organic carbon contents (corrected for porosity). C_{org} burial is thus linearly related to sediment accumulation, which in turn is approximately linearly related to sediment delivery to the ocean in the absence of major changes in sea level (Berner, 1982). Other factors governing C_{org} burial (e.g. oxygen) are secondary to sediment deposition (Hedges and Keil, 1995). Therefore, we focus our modelling efforts on linear astronomical forcing of C_{org} burial as a starting point. Since the model does not resolve shallow versus deep C_{org} burial, we force the long-term balance between burial and oxidation of C_{org} directly, without implying which particular mechanism is responsible.

Previous modelling studies have attempted to unravel the origin of the 405 kyr cyclic patterns found in Cenozoic $\delta^{13}\text{C}$ and $\delta^{18}\text{O}$ records. Pälike et al. (2006) hypothesized that the cycles are driven by variations in marine biosphere productivity in response to changes in insolation. Ma et al. (2011), however, focused their simulations on the effects of increased weathering with eccentricity maxima, resulting in increased inorganic carbon input in the oceans, which, in combination with higher nutrients, leads to increased productivity and ultimately increased C_{org} burial, coinciding with minima in global exogenic

$\delta^{13}\text{C}$. Paillard (2017), in a study on Pleistocene glacial-interglacial variability, argued that silicate weathering alone could not simultaneously account for the large $\delta^{13}\text{C}$ changes and the small $p\text{CO}_2$ changes, while nutrient or ecology-induced changes in C_{org} burial would not result in a change to these cycles during the onset of glaciations. Therefore Paillard (2017) focused on monsoon-driven changes in C_{org} burial, which may be similar to our approach – as the monsoonal changes lead to changes in precipitation, which cause an increased riverine clay flux, resulting in increased C_{org} burial. Zeebe et al. (2017) forced C_{org} burial in marine sediments directly with various orbital forcing scenarios and noise, to understand a sediment record from the Paleocene and Eocene. These and previous modelling studies demonstrate how high-frequency spectral power in input forcing is shifted to lower frequencies (Pälike et al., 2006; Ma et al., 2011; Zeebe et al., 2017) dampened, resulting in increased power in the lower frequencies (Pälike et al., 2006; Ma et al., 2011; Paillard, 2017; Zeebe et al., 2017); The long residence time of carbon in the oceans (Broecker and Peng, 1982) effectively filters the input signal, resulting in a strongly muted response on short time scales, which allows only the lowest frequencies in the input forcing to become apparent in the record.

The question remains if this shifting of spectral power to lower frequencies low-pass filtering also affects the much longer 2.4 Myr eccentricity cycle, for which indications have been found in geological records for the Eocene (Lourens et al., 2005), Paleocene (Westerhold et al., 2011), Oligocene (Pälike et al., 2006; Valero et al., 2014), and Miocene (Holbourn et al., 2007; Liebrand et al., 2016). The 2.4 Myr cycle is present in the astronomical solution as both an amplitude modulator (AM) of the 124 and 95 kyr eccentricity cycles as well as a true eccentricity cycle and is caused by orbit–orbit resonance between Mars and Earth ($g_4 - g_3$) (Laskar et al., 2011). This cycle is never unambiguous in palaeoclimate records, because long time series are required and the long period of this cycle overlaps with the time scale of slow tectonically-driven climate change (>1 Myr), and can therefore be obscured by the latter. The signal can also be lost when data are detrended prior to spectral analyses.

Here we aim to investigate the general role of eccentricity forcing on the carbon cycle across the Cenozoic, and specifically provide a model–data comparison with Oligocene and Miocene carbon isotope records. ~~The continental shelves provide the largest C_{org} storage potential over astronomical time scales, therefore we~~ We linearly force C_{org} burial in marine sediment with astronomical forcing in this modelling study, to assess the response of the carbon cycle. ~~We choose to force the long-term balance between burial and oxidation of C_{org} directly, without implying which particular mechanism is responsible.~~

25 2 Material and Methods

We investigate the response of the carbon cycle to variations in orbital parameters by conducting a modelling study with simple linear forcing of organic carbon burial, using the Long-term Ocean-atmosphere-Sediment Carbon cycle Reservoir model (LOSCAR, Zeebe, 2012). In the model, C_{org} burial and weathering were forced with various aspects and combinations of the orbital solution by Laskar et al. (2004). We use spectral analysis techniques to study cyclic patterns in the model output. Finally, we compare modelling results to a long-term high-resolution data composite of published benthic foraminiferal isotope records from the Pacific Ocean.

2.1 LOSCAR model

The LOSCAR model simulates and tracks changes in the partitioning of carbon throughout the ocean basins, sediments and atmosphere over both short (centuries) and long (millions of years) time scales (Zeebe, 2012). The model consists of a number of easily adjustable ocean boxes: in the set-up used here, it comprises an atmosphere, the Atlantic, Indian, and Pacific oceans, each with a surface-, intermediate-, and deep box, and one general high-latitude surface ocean box. All oceans are coupled to a prescribed number of sediment boxes (13 for each ocean here). A thermohaline circulation is imposed in the model by way of flow-rates between specific ocean boxes. Various tracers (e.g. dissolved inorganic carbon (DIC), $p\text{CO}_2$, pH, and the $\delta^{13}\text{C}$, as well as the ~~diagnostic~~-carbonate compensation depth (CCD)) are tracked for the different ocean boxes in the model through time.

Carbon cycling in the model operates on various time scales that are relevant here, including volcanism and the long term weathering feed-backs, and the short-term gas exchange (similar to Berner et al., 1983). Long-term carbon cycling is implemented in the model as a flux of volcanic degassing and metamorphic processes (F_{vc}^0) and weathering of organic matter from the rock reservoir (F_{OC}^{in}), with atmospheric CO_2 being consumed by carbonate weathering (F_{cc} , Reaction R1) and silicate weathering (F_{si} , Reaction R2).



These weathering reactions respond as a negative feedback to variations in the CO_2 concentration as follows:

$$F_{cc} = F_{cc}^0 \left(\frac{p\text{CO}_2}{p\text{CO}_2^0} \right)^{n_{cc}} \quad (1)$$

$$F_{si} = F_{si}^0 \left(\frac{p\text{CO}_2}{p\text{CO}_2^0} \right)^{n_{si}} \quad (2)$$

Where F_{cc} and F_{si} are the carbonate and silicate weathering fluxes respectively, the superscript “0” refers to initial (steady-state) value of the weathering flux and CO_2 respectively. The n_{cc} and n_{si} parameters control the strength of the weathering feedback. Steady state is reached when the silicate weathering flux balances the CO_2 degassing flux from volcanism, i.e. $F_{si} = F_{vc}$. These are all slow processes, where the steady-state balance is restored after a perturbation on time scales in the order of 10^5 to 10^6 yr (Zeebe, 2012).

Carbon cycling also occurs on a much more rapid time scale in the oceans and atmosphere through the biological pump, air-sea exchange and remineralisation of carbon. In the original LOSCAR model (version 2.0.4), the biological pump is decoupled

from the long carbon cycle described above, meaning that C_{org} that is produced in surface oceans is fully remineralised in the intermediate and deep ocean boxes (see Zeebe, 2012, for a full description). We note that Komar and Zeebe (2017) included a long-term, coupled C_{org} - O_2 - PO_4 feedback in LOSCAR. However, a simplified approach is used here (see below), since our simple forcing does not invoke additional controls on C_{org} burial, such as productivity.

5 2.2 Orbital forcing

We spun up the modern (i.e. post-Paleocene–Eocene) set-up of LOSCAR with atmospheric CO_2 concentrations of 450 ppmv with default parameter values listed in Zeebe (2012) for 10 Myr. Initial CO_2 concentrations of 450 ppmv are roughly consistent with averaged late Paleogene to Neogene proxy estimates (e.g. Foster et al., 2012; Zhang et al., 2013)(e.g. Foster et al., 2012; Zhang et al., . The equilibrium was then perturbed by linear scaling of the C_{org} burial rate with the orbital forcing signal at each time step (Eq. 3), with higher burial occurring with weaker forcing (F_{inp} , some form of ETP, eccentricity, insolation, or clipped insolation).

$$Z = \frac{F_{inp} - \min F_{inp}}{\max F_{inp} - \min F_{inp}} \quad (3)$$

$$F_{orb} = 2(Z - \bar{Z}) \quad (4)$$

$$F_{gb} = F_{gb}^0(1 - \alpha F_{orb}), \quad (5)$$

15 where Z is the input forcing, F_{inp} , scaled between 0 and 1. The scaled orbital forcing, F_{orb} , is Z minus its mean value, \bar{Z} , multiplied by 2 so that it is scaled between -1 and 1 . F_{gb} is the C_{org} flux resulting from the initial steady-state C_{org} flux, F_{gb}^0 , being scaled with adjustable parameter α and F_{orb} . Thus, weaker input forcing is associated with increased burial, which in nature could be explained by ~~increased clay delivery, formation~~ if weathering is not limiting (Sect. 1) – increased clay formation, delivery, and deposition, and associated burial of C_{org} .

20 To force these changes in C_{org} burial, different combinations of the orbital parameters can be used. F_{inp} ~~consists of~~ was implemented as eccentricity or precession separately, or as artificial combinations of eccentricity, obliquity (tilt) and precession (together ETP), ~~and which~~ is created by normalizing (subtracting the mean, then dividing by the standard deviation) and adding the ETP components, after scaling them with different factors. Forcing the model with individual components and ETP may seem rather artificial but allows us to study the impact of individual orbital components, and infers no mechanistic
25 understanding of the underlying processes – such as the position of deep water formation ~~– and could hence be considered more objective than the use of e.g. seasonal insolation at a specific latitude.~~ We also force with various insolation schemes with different latitudes and seasons.

To test the robustness of the carbon cycle response to changes in orbitally-forced C_{org} burial, a parameterized amount of white noise (scaled between -1 and 1) was added to the burial rate. Noise was generated and applied when a time interval
30 larger than 1 kyr since the previous noise addition had passed. As additional sensitivity analyses, several (newly introduced) model parameters were changed to study their effect on model output. The atmospheric CO_2 concentration, the impact of the

forcing on the C_{org} burial (α), the ~~relative makeup of the ETP curve (also simulating 65° N summer insolation, which required artificial clipping to shift spectral power to the eccentricity components),~~ the amount of noise, as well as the time step after which noise was added were adjusted to find how these affect model output. When using ETP as forcing, the relative make-up of the ETP curve, was varied, while for summer insolation different ways of artificial clipping were applied so as to simulate a non-linear response resulting in increased spectral power in the eccentricity components.

2.3 Data compilation

A high resolution (22 Myr long, 34 to 12 Ma, median sampling interval of 4 kyr) composite record of benthic foraminiferal $\delta^{13}C$ and $\delta^{18}O$ (Fig. 1) was compiled using data from Ocean Drilling Program (ODP) Leg 199 Site 1218 (8°53.378'N, 135°22.00'W, 4.8 km water depth, Pälike et al. (2006)) and Integrated ODP (IODP) Site U1337 (3°50.009'N, 123°12.352'W, 4.2 km water depth, Tian et al. (2013); Holbourn et al. (2015)), located in the equatorial East Pacific (Fig. 1 (a)). We use records from the Pacific, because it represents the largest ocean reservoir by volume, and compare these to output from LOSCAR's Pacific box. Initial age models for the records were established from $^{40}Ar/^{39}Ar$ isotopes, planktonic foraminiferal-, nannofossil-, radiolarian-, and/or magnetostratigraphic datum events, and known ages of changes in wt % $CaCO_3$ contents. The age models of these records are based on similar dating and tuning strategies and we therefore assume that they are compatible for the purposes of this long-term study. Initial age models were subsequently improved through astronomical tuning to the orbital solution by Laskar et al. (2004). Pälike et al. (2006) tuned their record to an Eccentricity Tilt Precession (ETP) model (with ratio 1:0.5:−0.4) starting with the 405 kyr cycle and then moving on to the shorter astronomical frequencies, while Holbourn et al. (2015) tuned their $\delta^{18}O$ minima to ETP (1:1:0.2) maxima and Tian et al. (2013) tuned $\delta^{18}O$ minima to obliquity maxima (which represents the same phase relation).

Areas of overlap in the various records comprising the data composite were checked for consistency in phase relationship, absolute value (~~see digital supplement~~ Supp. Sect. 3) and amplitude variation. The $\delta^{13}C$ and $\delta^{18}O$ composite data from Pälike et al. (2006) were limited to the higher-resolution range between 20 to 34 Ma to keep the resolution comparable to the other records. Due to minor inconsistencies in the two age models for site U1337, data from Tian et al. (2013) were excluded in the overlapping depth region because of the lower resolution and shorter record length compared to the Holbourn et al. (2015) record.

2.4 Spectral analysis

All analyses were performed using the R programming language (R Core Team, 2018), including various functions of the Astrochron package (Meyers, 2014), unless indicated differently. To identify periodicity in both the model output and the data composite, the multitaper method (MTM) by Thomson (1982) was applied. First, data and model output were linearly re-sampled to the median sampling interval of the data composite (4 kyr). For the MTM-analysis, two tapers were used and the data or model output were zero-padded with a length of five times the input length. The data composite was also filtered for periods larger than 3.1 Myr to remove longer-scale climate trends that likely have causes other than orbital forcing, to allow for easier model–data comparison of records and spectra. The value of 3.1 Myr was chosen based on a small trough

in spectral output of the raw data composite around this value (Sect. 3). This was achieved by applying a low-pass filter (for periods below 3.1 Myr), subtracting this signal from the original composite and re-adding the mean of the low-passed signal. Cross-correlation was performed between model-output and input forcing, to estimate phase-lags and provide insight into the dominant mechanisms determining model response to orbital forcing of C_{org} -burial. This was achieved with the Blackman-
5 Tukey method, using a Bartlett window, using 30 % of the series, with a time-step of 1×10^{-5} cycles/kyr using Analyseries 2.0.8 (Paillard et al., 1996). Amplitude modulation of shorter cycles was investigated by filtering for the short eccentricity cycles ($0.010 \pm 0.003 \text{ kyr}^{-1}$), performing a Hilbert transform which connects all the peaks in the record, and applying the MTM on the result (adapted from Zeebe et al., 2017). To evaluate how the frequency distribution and amplitude modulation changes through time in the composite record, evolutive multitaper harmonics analysis (EHA) was performed on the 1 Myr
10 negative filtered composite of $\delta^{13}\text{C}$ using a time step of 50 kyr and a window size of 0.7 Myr (similar to Pälike et al., 2006; Liebrand et al., 2016).

3 Results and Discussion

3.1 Model output

All tracers in the model output show cyclic alternations as a result of implementing astronomical forcing of C_{org} burial in
15 the model (Fig. 2 [and Supp. Fig. 10 for all model output](#)). Model tracers do not show much inter-basin variability, thus we will consider the deep Pacific box (DP) to assess the generalized oceanic behaviour of tracers. ~~The~~ [As expected, the](#) total exogenic carbon inventory C_{tot} in the ocean basins closely matches changes in atmospheric CO_2 , dissolved inorganic carbon (DIC) and temperature. While the carbonate compensation depth (CCD) of the DP shows cyclic extreme outliers due to model design (~~see digital supplement~~ [Supp. Sect. 1](#)), the underlying pattern of change is also similar, with high temperatures, high
20 CO_2 concentrations, and high C_{tot} co-occurring with a deepening of the CCD for the 405 kyr and 2.4 Myr cycles. DP $\delta^{13}\text{C}$ co-varies approximately in anti-phase (i.e. ^{13}C -depleted DIC co-occurring with high C_{tot}) with these tracers but shows more higher-frequency fluctuations.

The MTM-analysis of model output shows significant spectral power at orbital periods (Fig. 3). Most notably, ~~a shift in~~ [decreased](#) spectral power occurs ~~from in~~ the higher frequencies (precession, obliquity) in the forcing signal ~~to~~, [while](#) the
25 lower frequencies (long-term eccentricity cycles), that are sometimes only marginally present in the input forcing ~~. The shift in~~ [spectral power to lower frequencies in the input forcing gain spectral power. This low-pass filtering of spectral power,](#) occurs for our main scenario of 1:0.5:−0.4 ETP, but also for various other combinations of ETP (e.g. 1:0.5:−0.4, 0.1:0:0.1, 1:1:1, etc.), eccentricity alone, and unclipped/clipped 65°N [and 30°N](#) summer insolation (~~see digital supplement~~ [Supp. Sect. 4](#)). Results are qualitatively similar for different contributions of E, T, and P in the ETP curve as forcing. Furthermore, the results are largely
30 unaffected by the introduction of relatively strong ~~noise that~~ [white noise, that is transformed into red noise, that](#) affects C_{org} burial by up to the same levels as the astronomical forcing, and different initial modelling conditions. Together, these sensitivity studies indicate that the model results in terms of spectral response are very robust ([Supplement Supp. Sect. 4](#)).

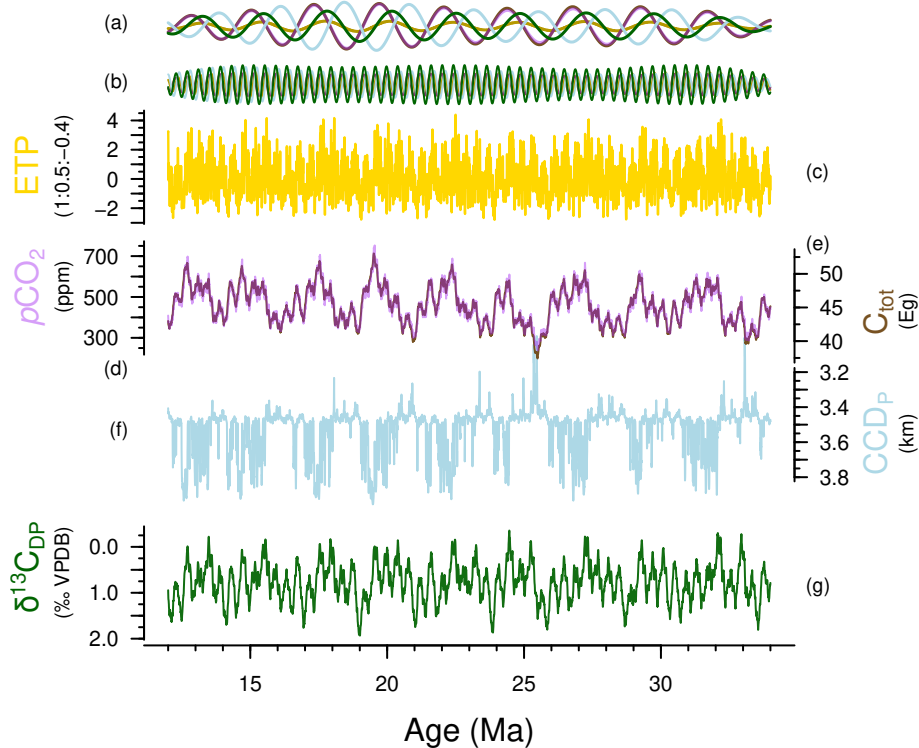


Figure 2. LOSCAR model output time series for orbitally-forced carbon burial with orbital forcing strength $\alpha = 0.5$ and noise level 0.2. (a) 405 kyr (frequency of $2.46 \pm 0.15 \text{ Myr}^{-1}$) and (b) 2.4 Myr ($0.42 \pm 0.15 \text{ Myr}^{-1}$) bandpass filters are shown (same colours, arbitrary y-axis). (c) The ETP (1:0.5:−0.4) construct used as orbital forcing in this scenario (gold). (d) The Atmospheric CO₂ (purple, parts per million volume, ppm) and (e) the total exogenic carbon inventory (brown, Eg (10^{18} g)). (f) Pacific carbonate compensation depth (CCD) (blue, km, note the cutoff y-axis due to large outliers, explained in Supp. Sect. 1) (g) Deep Pacific δ¹³C (green, ‰ Vienna Pee Dee Belemnite (VPDB), reversed axis). Atmospheric CO₂ (parts per million volume (ppmv)), deep Deep Pacific temperature (°C), and Dissolved Inorganic Carbon (DIC) of the Deep Pacific model output are omitted from this plot, because their pattern mirrors that of C_{tot} and pCO₂ (Supp. Fig. 10).

By comparing the dominant frequencies in our output to the characteristic frequencies of orbital solution from Laskar et al. (2004), the corresponding orbit–orbit resonances between the planets were found (Digital-supplementSupp. Table 1). Surprisingly, the 2.4 Myr cycle in carbon and oxygen isotopes is strongly present in the model output (including DIC, atmospheric CO₂, deep Pacific temperature and C_{tot}). The other strong eccentricity cycles consist of a 1 Myr cycle that is related to a

5 Mercury–Jupiter ($g_1 - g_5$) resonance, and the 405 kyr cycle that is related to Venus–Jupiter ($g_2 - g_5$).

Interestingly, the shifting of spectral power to lower frequencies low-pass filtering occurs differently for the different tracers. The DIC, atmospheric CO₂, C_{tot} and temperature show very high relative dominance of the long eccentricity cycles (2.4, 1 and 0.7 Myr), while δ¹³C – and to a lesser extent CCD – show more spectral power in the shorter eccentricity range (405, 127 and 95 kyr) (Fig. 3). To investigate why spectral power is differentially shifted-filtered differently for these tracers, residence

Table 2. Calculated residence times of the main carbon cycle processes.

Process	Reservoir / Flux	Residence time
SiO ₂ weathering	TCO ₂ / F_{si}	655 kyr
CaCO ₃ weathering	TCO ₂ / F_{cc}	280 kyr
Carbonate compensation	TCO ₃ ²⁻ / F_{cc}	10 kyr

times were calculated for the key carbon cycle feedbacks in the model by dividing the reservoir sizes by the respective fluxes (See Table 2). Silicate weathering, with a residence time of 655 kyr, is the slowest feedback system in our model. Carbonate weathering operates on timescales of the same order of magnitude (280 kyr), while oceanic carbonate compensation is an order of magnitude faster (10 kyr). This means that silicate weathering ~~is most capable of shifting spectral power to the~~ most strongly

5 low-pass filters the spectral power, resulting in a dominant 2.4 Myr eccentricity cycle.

The $\delta^{13}\text{C}$ gradients of carbon in the oceans are modulated by changes in the (^{13}C -depleted) C_{org} pump. The biological pump operates much more rapidly than silicate- and carbonate weathering, but remains constant in the model. Therefore, changes in the $\delta^{13}\text{C}$ gradients are dominated by the total C_{org} inventory, on which we directly impose our forcing.

3.1.1 Phase relations of model tracers

10 Cross-spectral analysis between the key carbon cycle tracers in the model output and the ETP-forcing reveals different phasing for the various tracers, as well as for the different time-scales under consideration (Fig. 4). A phase of 0° implies that the ~~variable-tracer~~ is changing exactly in phase with the ETP-forcing, while at 180° or -180° they are ~~precisely out of phase in~~ anti-phase. Positive (negative) values indicate that the variable is lagging (leading) with respect to the ETP-forcing.

Broadly, we observe that phasing remains rather constant for each tracer for periods <405 kyr, while absolute lag-time
15 decreases as a function of frequency (Supplementary-Supp. Fig. 7). The atmospheric CO₂ concentration and ocean temperature show the smallest lags – or fastest response – compared to the oceanic tracers. This is because the much shorter residence time of CO₂ in the atmosphere (in the order of several years) – due to its relatively small reservoir size and fast cycling – causes atmospheric CO₂ concentrations to respond rapidly to changes in sea surface carbon. The fast temperature response occurs because ocean temperature change propagates at a ~~faster~~ higher rate than changes in ocean chemistry. Atmospheric CO₂ and
20 ocean temperature therefore appear to be in quasi-steady state with respect to the other tracers in the model. ~~The total carbon inventory (C_{tot}, pCO₂ + DIC) operates in phase with the ocean tracers, which reflects that the DIC-pools across the oceans are much larger than the atmospheric reservoir.~~ Furthermore, cycling in the deep (D) and intermediate (I) Pacific (P) boxes is slower than the low-latitude surface (L) boxes for DIC. This is also a result of relative reservoir size and air-sea exchange. The CCD has a negative phase for the higher frequencies (precession, obliquity, and 100 kyr eccentricity), indicating anti-phasing
25 relative to the other tracers. With ETP-maxima, the CCD shoals at these shorter time-scales due to relatively rapid carbonate

compensation as a short-term response to increased atmospheric CO₂ (Table 2). On longer time-scales (>100 kyr), however, the CCD shifts to in-phase cycling – deepening of the CCD with ETP-maxima – as a result of increased weathering and increased riverine input of DIC and TA, which increases the oceanic DIC inventory but also restores alkalinity to the ocean.

~~The For the phase-analysis was performed such that $\delta^{13}\text{C}$ minima are phased with, $\delta^{13}\text{C}$ minima were compared to~~ ETP maxima (i.e. $-\delta^{13}\text{C}$ was ~~used compared to ETP~~), while the other tracers (CCD, C_{tot}, CO₂) were not adjusted. The high-frequency range shows similar lags to the DIC and C_{tot}. Surprisingly, the DP box shows a slightly faster response than the LP and IP boxes, in fact more akin to the atmospheric reservoir for the precession frequencies. With decreasing frequency (i.e. the 405 kyr to 2.4 Myr eccentricity components), this relation between the deep and shallower boxes switches and the $-\delta^{13}\text{C}$ starts to lag more and more, reaching an overshoot of more than half a period for the 2.4 Myr cycle in the DP box, causing the 2.4 Myr-cycle in $-\delta^{13}\text{C}$ to appear as leading the signal in the ETP-forcing (~~Supplement-Supp.~~ Fig. 2). This can be demonstrated to be an overshoot response (~~digital-supplement-??~~ [Supp. Sect. 5](#)). It is also interesting to note that $\delta^{13}\text{C}$ leads over DIC. This is because the DIC-response is determined by ocean chemistry and thus weathering, whereas the $\delta^{13}\text{C}$ -signal is mostly influenced by residence time and C_{org} cycling.

3.2 Data composite

The composite record consists of a carbon isotope record of relatively high resolution (median sampling interval of ~4 kyr), spanning the Oligocene and most of the Miocene (34 to 12 Ma). However, there is a lower resolution stretch of data between 20.0 and 21.5 Ma (Fig. 1). The highest and lowest (Nyquist and Rayleigh) detectible frequencies are thus $F_N = 1/(2\Delta t) = 0.125 \text{ kyr}^{-1}$ and $F_R = 1/(N\Delta t) = 0.046 \text{ Myr}^{-1}$ respectively.

The dominant frequencies in the data composite correspond to the main orbital periods of eccentricity (405, 124 and 95 kyr), obliquity (41 kyr), and precession (23, 22 and 19 kyr) (Fig. 5), similar to the results of the individual records (Pälike et al., 2006; Tian et al., 2013; Holbourn et al., 2015). Despite detrending, very high spectral power remains in the very low frequency range (~~<0.5 Myr~~ [<0.5 Myr⁻¹](#)) (Fig. 5 (c)). This could be caused by non-periodic long-term climatic variations, or possibly by bundles of 2.4 Myr cycles (Boulila et al., 2012).

The dominant 2.4 Myr cyclicity observed in our model output seems absent in the $\delta^{13}\text{C}$ composite record when performing MTM spectral analysis. ~~This indicates that the 2.4 Myr cycle acts purely as an amplitude modulator (AM) on the other eccentricity cycles in the composite record, and not as a true cycle.~~ The EHA records a strong influence of the 405, 127 and 95 kyr cycles throughout the composite record, which vary in intensity over 2.4 Myr intervals (Fig. 6). Furthermore, the envelope of the 100 and 405 kyr filtered record also ~~reflects AM by the longer eccentricity cycles~~ ([Supplement changes at 2.4 Myr intervals](#) (Supp. Fig. 8). [This indicates that the 2.4 Myr cycle acts purely as an amplitude modulator \(AM\) on the other eccentricity cycles in the composite record, and not as a true cycle.](#)

As a true cycle, the 2.4 Myr signal may be overshadowed by spectral power in the lower-frequencies (Fig. 5). If these are filtered out (periods <3.1 Myr, red shaded region in Fig. 5 (c)), the AR-1 fit and 95 % confidence levels are lowered on the low-frequency range (<20 Myr⁻¹), but spectra are unaffected. The relatively high spectral peak in the 2.4 Myr range of the low-pass filtered data composite is therefore interpreted to be a combined result of a weak (overshadowed) signal in the data,

and an artefact produced by cutting off (low-pass filtering) the even lower frequencies, leaving only this frequency range in the spectral outcome. The obliquity and precession components also change through time, but contribute less power to the EHA-spectrum. Qualitatively, a weak 1 Myr bundling can be inferred for these frequencies, especially for the older range (25 to 34 Ma). This could be related to the ~ 1 Myr obliquity cycle.

5 3.3 Model–data comparison

The model generates quite comparable time series to the high-passed data composite in terms of amplitude, phasing, and associated spectra. The distribution of spectral power in astronomical components is similar, and can be matched to fit the data composite more closely by adjusting the strength of the orbital forcing, the make-up of the ETP, or the noise level (Supplement Sect. 4). However, while the 2.4 Myr eccentricity cycle is predominantly present as a true cycle in the model output, the composite record instead contains a strong presence of this cycle as amplitude modulator of the shorter eccentricity cycles. ~~The mechanism by which the 2.4 Myr cycle functions as an AM on the other low-frequency ranges in the data composite is thus not captured in the model, as evidenced by the absence of bundling of eccentricity periods in the EHA of model output (Supplement~~ Upon further inspection, we also find ~ 2.4 Myr bundling of the short eccentricity cycles in the EHA of model output (Supp. Fig. 9. This is probably the result of the eccentricity component in the ETP, as this bundling is absent when forcing with, e.g. 65°N summer insolation. The changes in temperature ($\sim 3^\circ\text{C}$) that were calculated from model output CO_2 (Supp. Fig. 10) are larger than the temperature estimates based on the $\delta^{18}\text{O}$ composite data (which would be $\sim 1^\circ\text{C}$). This is because the carbon cycle model (not a climate model) relates temperature to CO_2 directly through an input climate sensitivity of 5°C per CO_2 doubling, whereas in reality temperature is a function of a number of variables, including but not limited to $p\text{CO}_2$. For example, insolation directly affects the climate system components (e.g. atmosphere, etc.), which in turn affect temperature. These insolation-driven changes to the climate system are not part of the temperature-response to $p\text{CO}_2$, however. This behaviour cannot be captured by the carbon cycle model. In addition, this climate sensitivity strongly depends on the strengths of various feedbacks at various time scales, which likely also vary through time (e.g., Rohling et al., 2012; von der Heydt et al., 2016). The lack of a strong 2.4 Myr cycle in $\delta^{18}\text{O}$ records (and its associated temperature) therefore does not necessarily imply that the 2.4 Myr cycle cannot be dominant in $p\text{CO}_2$.

Unfortunately, even the available $p\text{CO}_2$ records for the Pliocene–Pleistocene (e.g., Bartoli et al., 2011; Seki et al., 2010) are of insufficient resolution (~ 200 kyr, potential for aliasing) and duration (~ 5 Myr, at best 2 cycles) to test for a 2.4 Myr cycle. Furthermore, potentially cyclic changes could be overshadowed due to proxy uncertainty. New, long $p\text{CO}_2$ proxy records are required to establish a possible 2.4 Myr cyclicity. Since the resulting model $p\text{CO}_2$ can be adjusted by changing input parameters of forcing, noise, etc. (Supp. Sect. 4), comparison in terms of absolute values is not meaningful.

On long time-scales, the model’s CCD output can be compared to reconstructions of the Pacific CCD based on CaCO_3 accumulation rates (CAR) from various sites (Pälike et al., 2012). These records indicate a deep and stable CCD during the Oligocene–Miocene up to about 18.5 Ma, but our modelled CCD depth is highly variable on 405 kyr and 2.4 Myr time-scales – ranging from ~ 10 to 100 m if we exclude model-setup-induced outliers (Supp. Sect. 1). The CCD reconstructions for the Eocene, however, are highly variable on these time-scales (changing by up to ~ 500 m) and potentially show indications for

long-term eccentricity-forced cycles. We performed spectral analyses on the CAR for the different sites as well as the inferred Pacific CCD (Supp. Figs. 1 and 2). In these records, long-term trends and step changes, are controlled by long-term non-cyclic forcings such as volcanism, sea level or long-term changes in the climate (Pälike et al., 2012). Therefore, we remove the long-term trend using a loess-fit prior to spectral analysis. These analyses provide some evidence for 2.4 Myr cyclicality in the longest continuous CAR records for Site 1333 and Site 1334 (Supp. Fig. ??, also with EHA of 65° N summer insolation and a similar ETP construct), 1) as well as for the global CCD reconstruction (Supp. Fig. 2). The evidence is far from strong, however, because also these records are of low resolution – insufficient to resolve the short (100 and 405 kyr) eccentricity cycles and certainly precession. Furthermore, there are indications that the 2.4 Myr eccentricity cycle that is present in the astronomical solution is expressed as a 1.2 Myr AM of the short eccentricity cycle during the Eocene, due to either a resonance with, or a non-linear response of the residence time of gas hydrates (Galeotti et al., 2010), further complicating the matter. The fact that we see some evidence for the 2.4 Myr cycle, given these caveats, however, is noteworthy.

The phasing of the model and data records differ in terms of absolute lag (kyr): the modelled $\delta^{13}\text{C}$ response is overall slower compared to data records. For example, the lag of $\delta^{13}\text{C}$ to the 405 kyr eccentricity cycle is ~ 190 kyr, which is much higher than the 40 to 60 kyr during estimates for the Paleocene (Westerhold et al., 2011) and 20 to 30 kyr during the Oligocene (Pälike et al., 2006). Of course the lag times of data records are calculated after the tuning of a record, and are therefore likely underestimated. However, the large difference between modelled lag-times and lag-times calculated from tuned records may indicate a lack of understanding regarding the underlying mechanisms.

With simple linear C_{org} burial forcing using an artificial combination of eccentricity, precession and tilt, we are able to generate a $\delta^{13}\text{C}$ profile for the Eocene–Miocene that is very comparable to a long term high-passed data composite (Fig. 5) in both the time (Fig. 2) and frequency domains (Fig. 3). This indicates that cyclic burial of C_{org} at continental margins should be considered as a potential candidate driving $\delta^{13}\text{C}$ and $\delta^{18}\text{O}$ variability on eccentricity time scales.

3.4 Outlook

Looking forward, we could utilise phase-lag results of modelling studies to further constrain the lag between astronomical forcing and sedimentary records, allowing for an even more precise absolute astronomical tuning. Currently, most studies assume no phase-lag between astronomical forcing and the palaeorecord due to lack of absolute ages relative to the astronomical solution.

Future work could focus on evaluating the different magnitudes of the spectral power shifts-changes towards lower frequencies between different carbon cycle variables in the palaeorecord, as modelled $\delta^{13}\text{C}$ of C_{org} shows a less-pronounced shift in spectral power dampening of high-frequencies compared to other model tracers such as the CCD, total exogenic carbon, temperature or atmospheric CO_2 . Ideally this would require high-resolution records (at least $5\times$ the Nyquist frequency for the period of interest, i.e. every 2.3 kyr if we want in order to resolve precession) long-term (ideally >5 2.4 Myr cycles, 12 Myr) records for various climate variables, and could prove quite a challenge.

4 Conclusions

The carbon cycle box model simulations presented here reveal that simple orbital forcing of organic carbon burial in the ocean can reproduce the dominant 405 kyr cycle that is observed in Cenozoic carbon isotope records. The good correspondence between modelled carbon isotopes and the palaeorecord confirms orbitally forced burial of organic carbon ~~on the continental~~
5 ~~margins~~ as a possible candidate for causing the observed 405 kyr cyclicity in $\delta^{13}\text{C}$.

The link between astronomical forcing, carbon cycle dynamics, and the climate system that may give rise to this consistent eccentricity-forced periodicity is still poorly understood. Here we show that astronomical forcing of C_{org} burial in the marine realm could be a mechanism that explains this link in both a glaciated and ice-free world. As C_{org} burial is primarily controlled by sediment accumulation (~~Hedges and Keil, 1995; Berner, 2006~~) (Berner, 1982; Hedges and Keil, 1995; Berner, 2006)
10 , the direct top-down control for C_{org} burial ~~on continental margins~~ would be river runoff, which corresponds to seasonal precipitation patterns (see also Paillard, 2017; Zeebe et al., 2017). Although the exact mechanistic link between eccentricity forcing and sediment deposition remain elusive, we demonstrate that marine C_{org} burial provides an alternative to other proposed mechanisms that link the carbon cycle to astronomical forcing, such as carbon storage in peat-land soils (Kurtz et al., 2003), methane hydrate reservoirs, or ice-sheet dynamics (de Boer et al., 2014).

15 Importantly, this modelling study implies a ~~large~~ significant role for the 2.4 Myr eccentricity cycle in modulating carbon cycle dynamics, especially in DIC and atmospheric CO_2 . The 2.4 Myr eccentricity cycle is also present in the data composite, but acts dominantly as an amplitude modulator of the 127 and 95 kyr eccentricity cycles, and to a lesser extent as a true cycle, possibly due to overshadowing by slower cycles. The hypothesis that the Cenozoic pCO_2 - pCO_2 spectrum was dominated by the 2.4 Myr eccentricity could be evaluated using long, high-resolution proxy records of pCO_2 - pCO_2 or other carbonate chemistry
20 parameters.

Code and data availability. The LOSCAR model source code is available upon request to loscar.model@gmail.com. The data that was used to create the data composite are available through the Pangaea database (<http://pangaea.de>).

Author contributions. Modelling work was conducted by MJC and IJK. Data compilation was generated by IJK. All authors provided feedback on the manuscript.

25 *Competing interests.* The authors declare that they have no conflict of interest.

Acknowledgements. IJK thanks the kfHein fund for financial support. MJC thanks the Molengraaff Fund for financial support. REZ was supported by U.S. NSF grants OCE12-20615 and OCE16-58023. This work used data generated on samples provided by the International

Ocean Discovery Program (IODP) and was carried out under the program of the Netherlands Earth System Science Centre (NESSC). We also thank Frits Hilgen for extensive discussions and two anonymous reviewers for their input on the manuscript.

References

- Bartoli, G., Hönisch, B., and Zeebe, R. E.: Atmospheric CO₂ decline during the Pliocene intensification of Northern Hemisphere glaciations, *Paleoceanography*, 26, 1–14, <https://doi.org/10.1029/2010PA002055>, 2011.
- Berner, R. A.: Burial of organic carbon and pyrite sulfur in the modern ocean: Its geochemical and environmental significance, <https://doi.org/10.2475/ajs.282.4.451>, 1982.
- Berner, R. A.: Inclusion of the weathering of volcanic rocks in the GEOCARBSULF model, *Am. J. Sci.*, 306, 295–302, <https://doi.org/10.2475/05.2006.01>, 2006.
- Berner, R. A., Lasaga, A. C., and Garrels, R. M.: The carbonate-silicate geochemical cycle and its effect on atmospheric carbon dioxide over the past 100 million years., <https://doi.org/10.2475/ajs.283.7.641>, 1983.
- 10 Boulila, S., Galbrun, B., Laskar, J., and Pälike, H.: A 9 myr cycle in Cenozoic $\delta^{13}\text{C}$ record and long-term orbital eccentricity modulation: Is there a link?, *Earth Planet. Sci. Lett.*, 317–318, 273–281, <https://doi.org/10.1016/j.epsl.2011.11.017>, <http://dx.doi.org/10.1016/j.epsl.2011.11.017><http://linkinghub.elsevier.com/retrieve/pii/S0012821X11006741>, 2012.
- Broecker, W. and Peng, T.-H.: Tracers in the sea, Lamont-Doherty Geological Observatory, Columbia University, 1982.
- de Boer, B., Lourens, L. J., and van de Wal, R. S. W.: Persistent 400,000-year variability of Antarctic ice volume and the carbon cycle is revealed throughout the Plio-Pleistocene., *Nat. Commun.*, 5, 2999, <https://doi.org/10.1038/ncomms3999>, <http://www.ncbi.nlm.nih.gov/pubmed/24385005>, 2014.
- 15 Dean, J. F., Middelburg, J. J., Röckmann, T., Aerts, R., Blauw, L. G., Egger, M., Jetten, M. S. M., de Jong, A. E. E., Meisel, O. H., Rasigraf, O., Slomp, C. P., in 't Zandt, M. H., and Dolman, A. J.: Methane feedbacks to the global climate system in a warmer world, *Rev. Geophys.*, pp. 1–44, <https://doi.org/10.1002/2017RG000559>, <http://doi.wiley.com/10.1002/2017RG000559>, 2018.
- 20 Dickens, G. R.: Rethinking the global carbon cycle with a large, dynamic and microbially mediated gas hydrate capacitor, *Earth Planet. Sci. Lett.*, 213, 169–183, [https://doi.org/10.1016/S0012-821X\(03\)00325-X](https://doi.org/10.1016/S0012-821X(03)00325-X), 2003.
- Dickens, G. R.: Down the Rabbit Hole: Toward appropriate discussion of methane release from gas hydrate systems during the Paleocene-Eocene thermal maximum and other past hyperthermal events, *Clim. Past*, 7, 831–846, <https://doi.org/10.5194/cp-7-831-2011>, 2011.
- Foster, G. L., Lear, C. H., and Rae, J. W. B.: The evolution of pCO₂, ice volume and climate during the middle Miocene, *Earth Planet. Sci. Lett.*, 341–344, 243–254, <https://doi.org/10.1016/j.epsl.2012.06.007>, <http://dx.doi.org/10.1016/j.epsl.2012.06.007>, 2012.
- 25 Galeotti, S., Krishnan, S., Pagani, M., Lanci, L., Gaudio, A., Zachos, J. C., Monechi, S., Morelli, G., and Lourens, L.: Orbital chronology of Early Eocene hyperthermals from the Contessa Road section, central Italy, *Earth Planet. Sci. Lett.*, 290, 192–200, <https://doi.org/10.1016/j.epsl.2009.12.021>, <http://dx.doi.org/10.1016/j.epsl.2009.12.021>, 2010.
- Gradstein, F. M., Ogg, J. G., Schmitz, M., and Ogg, G., eds.: The Geologic Time Scale, Elsevier, <https://www.sciencedirect.com/science/article/pii/B9780444594259000019>, 2012.
- 30 Hedges, J. I. and Keil, R. G.: Sedimentary organic matter preservation: an assessment and speculative synthesis, *Mar. Chem.*, 49, 81–115, [https://doi.org/10.1016/0304-4203\(95\)00008-F](https://doi.org/10.1016/0304-4203(95)00008-F), 1995.
- Holbourn, A., Kuhnt, W., Schulz, M., Flores, J.-A., and Andersen, N.: Orbitally-paced climate evolution during the middle Miocene “Monterey” carbon-isotope excursion, *Earth Planet. Sci. Lett.*, 261, 534–550, <https://doi.org/10.1016/j.epsl.2007.07.026>, <http://linkinghub.elsevier.com/retrieve/pii/S0012821X07004736>, 2007.
- 35

- Holbourn, A., Kuhnt, W., Kochhann, K. G. D., Andersen, N., and Sebastian Meier, K. J.: Global perturbation of the carbon cycle at the onset of the Miocene Climatic Optimum, *Geology*, 43, 123–126, <https://doi.org/10.1130/G36317.1>, <http://geology.gsapubs.org/cgi/doi/10.1130/G36317.1>, 2015.
- Komar, N. and Zeebe, R. E.: Redox-controlled carbon and phosphorus burial: A mechanism for enhanced organic carbon sequestration during the PETM, *Earth Planet. Sci. Lett.*, 479, 71–82, <https://doi.org/10.1016/j.epsl.2017.09.011>, <http://linkinghub.elsevier.com/retrieve/pii/S0012821X17305071>, 2017.
- Kurtz, A. C., Kump, L. R., Arthur, M. A., Zachos, J. C., and Paytan, A.: Early Cenozoic decoupling of the global carbon and sulfur cycles, *Paleoceanography*, 18, <https://doi.org/10.1029/2003PA000908>, 2003.
- Laskar, J., Robutel, P., Joutel, F., Gastineau, M., Correia, a. C. M., and Levrard, B.: Astrophysics A long-term numerical solution for the insolation, *Astronomy*, 285, 261–285, <https://doi.org/10.1051/0004-6361>, <http://www.edpsciences.org/10.1051/0004-6361:20041335>, 2004.
- Laskar, J., Fienga, A., Gastineau, M., and Manche, H.: La2010: a new orbital solution for the long-term motion of the Earth, *Astron. Astrophys.*, 532, A89, <https://doi.org/10.1051/0004-6361/201116836>, <http://arxiv.org/abs/1103.1084><http://www.aanda.org/10.1051/0004-6361/201116836>, 2011.
- Lauretano, V., Littler, K., Polling, M., Zachos, J. C., and Lourens, L. J.: Frequency, magnitude and character of hyperthermal events at the onset of the Early Eocene Climatic Optimum, *Clim. Past*, 11, 1313–1324, <https://doi.org/10.5194/cp-11-1313-2015>, <http://www.clim-past.net/11/1313/2015/>, 2015.
- Liebrand, D., Beddow, H. M., Lourens, L. J., Pälike, H., Raffi, I., Bohaty, S. M., Hilgen, F. J., Saes, M. J. M., Wilson, P. A., Dijk, A. E. V., Hodell, D. A., Kroon, D., Huck, C. E., and Batenburg, S. J.: Cyclostratigraphy and eccentricity tuning of the early Oligocene oxygen and carbon isotope records from Walvis Ridge Site 1264, *Earth Planet. Sci. Lett.*, 1, 1–14, <https://doi.org/10.1016/j.epsl.2016.06.007>, <http://dx.doi.org/10.1016/j.epsl.2016.06.007>, 2016.
- Lourens, L., Sluijs, A., Kroon, D., Zachos, J. C., Thomas, E., Röhl, U., Bowles, J., and Raffi, I.: Astronomical pacing of late Palaeocene to early Eocene global warming events., *Nature*, 435, 1083–1087, <https://doi.org/10.1038/nature03814>, 2005.
- Lunt, D. J., Ridgwell, A., Sluijs, A., Zachos, J., Hunter, S., and Haywood, A.: A model for orbital pacing of methane hydrate destabilization during the Palaeogene, *Nat. Geosci.*, 4, 775–778, <https://doi.org/10.1038/ngeo1266>, <http://dx.doi.org/10.1038/ngeo1266>, 2011.
- Ma, W., Tian, J., Li, Q., and Wang, P.: Simulation of long eccentricity (400-kyr) cycle in ocean carbon reservoir during Miocene Climate Optimum: Weathering and nutrient response to orbital change, *Geophys. Res. Lett.*, 38, 1–5, <https://doi.org/10.1029/2011GL047680>, 2011.
- Matthews, K. J., Maloney, K. T., Zahirovic, S., Williams, S. E., Seton, M., and Müller, R. D.: Global plate boundary evolution and kinematics since the late Paleozoic, *Glob. Planet. Change*, 146, 226–250, <https://doi.org/10.1016/j.gloplacha.2016.10.002>, <http://dx.doi.org/10.1016/j.gloplacha.2016.10.002>, 2016.
- Meyers, S.: astrochron: An R Package for Astrochronology, CRAN, <http://cran.r-project.org/package=astrochron>, 2014.
- Paillard, D.: The Plio-Pleistocene climatic evolution as a consequence of orbital forcing on the carbon cycle, *Clim. Past*, 13, 1259–1267, <https://doi.org/10.5194/cp-13-1259-2017>, <https://www.clim-past.net/13/1259/2017/>, 2017.
- Paillard, D., Labeyrie, L., and Yiou, P.: Macintosh Program performs time-series analysis, *Earth Sp. Sci. News*, 77, 379, <https://doi.org/10.1029/96EO00259>, 1996.

- Pälike, H., Norris, R. D., Herrle, J. O., Wilson, P. A., Coxall, H. K., Lear, C. H., Shackleton, N. J., Tripathi, A. K., and Wade, B. S.: The heartbeat of the Oligocene climate system., *Science*, 314, 1894–8, <https://doi.org/10.1126/science.1133822>, <http://www.sciencemag.org/content/314/5807/1894.abstract>, 2006.
- Pälike, H., Lyle, M. W., Nishi, H., Raffi, I., Ridgwell, A., Gamage, K., Klaus, A., Acton, G., Anderson, L., Backman, J., Baldauf, J., Beltran, C., Bohaty, S. M., Bown, P., Busch, W., Channell, J. E., Chun, C. O., Delaney, M., Dewangan, P., Dunkley Jones, T., Edgar, K. M., Evans, H., Fitch, P., Foster, G. L., Gussone, N., Hasegawa, H., Hathorne, E. C., Hayashi, H., Herrle, J. O., Holbourn, A., Hovan, S., Hyeong, K., Iijima, K., Ito, T., Kamikuri, S. I., Kimoto, K., Kuroda, J., Leon-Rodriguez, L., Malinverno, A., Moore, T. C., Murphy, B. H., Murphy, D. P., Nakamura, H., Ogane, K., Ohneiser, C., Richter, C., Robinson, R., Rohling, E. J., Romero, O., Sawada, K., Scher, H., Schneider, L., Sluijs, A., Takata, H., Tian, J., Tsujimoto, A., Wade, B. S., Westerhold, T., Wilkens, R., Williams, T., Wilson, P. A., Yamamoto, Y., Yamamoto, S., Yamazaki, T., and Zeebe, R. E.: A Cenozoic record of the equatorial Pacific carbonate compensation depth, *Nature*, 488, 609–614, <https://doi.org/10.1038/nature11360>, <http://dx.doi.org/10.1038/nature11360>, 2012.
- R Core Team: R: A language and environment for statistical computing., <http://www.r-project.org/>, 2018.
- Rohling, E. J., Sluijs, A., Dijkstra, H. A., Köhler, P., Van De Wal, R. S., Von Der Heydt, A. S., Beerling, D. J., Berger, A., Bijl, P. K., Crucifix, M., Deconto, R., Drijfhout, S. S., Fedorov, A., Foster, G. L., Ganopolski, A., Hansen, J., Hönlisch, B., Hooghiemstra, H., Huber, M., Huybers, P., Knutti, R., Lea, D. W., Lourens, L. J., Lunt, D., Masson-Demotte, V., Medina-Elizalde, M., Otto-Bliesner, B., Pagani, M., Pälike, H., Renssen, H., Royer, D. L., Siddall, M., Valdes, P., Zachos, J. C., and Zeebe, R. E.: Making sense of palaeoclimate sensitivity, *Nature*, 491, 683–691, <https://doi.org/10.1038/nature11574>, <http://dx.doi.org/10.1038/nature11574>, 2012.
- Seki, O., Foster, G. L., Schmidt, D. N., Mackensen, A., Kawamura, K., and Pancost, R. D.: Alkenone and boron-based Pliocene pCO₂ records, *Earth Planet. Sci. Lett.*, 292, 201–211, <https://doi.org/10.1016/j.epsl.2010.01.037>, <http://dx.doi.org/10.1016/j.epsl.2010.01.037>, 2010.
- Thomson, D. J.: Spectrum estimation and harmonic analysis, *Proc. IEEE*, 70, 1055–1096, <https://doi.org/10.1109/PROC.1982.12433>, 1982.
- Tian, J., Yang, M., Lyle, M. W., Wilkens, R., and Shackford, J. K.: Obliquity and long eccentricity pacing of the Middle Miocene climate transition, *Geochemistry, Geophys. Geosystems*, 14, 1740–1755, <https://doi.org/10.1002/ggge.20108>, <http://doi.wiley.com/10.1002/ggge.20108>, 2013.
- Valero, L., Garcés, M., Cabrera, L., Costa, E., and Sáez, A.: 20 Myr of eccentricity paced lacustrine cycles in the Cenozoic Ebro Basin, *Earth Planet. Sci. Lett.*, 408, 183–193, <https://doi.org/10.1016/j.epsl.2014.10.007>, <http://www.sciencedirect.com/science/article/pii/S0012821X14006256>, 2014.
- von der Heydt, A. S., Dijkstra, H. A., van de Wal, R. S., Caballero, R., Crucifix, M., Foster, G. L., Huber, M., Köhler, P., Rohling, E., Valdes, P. J., Ashwin, P., Bathiany, S., Berends, T., van Bree, L. G., Ditlevsen, P., Ghil, M., Haywood, A. M., Katzav, J., Lohmann, G., Lohmann, J., Lucarini, V., Marzocchi, A., Pälike, H., Baroni, I. R., Simon, D., Sluijs, A., Stap, L. B., Tantet, A., Viebahn, J., and Ziegler, M.: Lessons on Climate Sensitivity From Past Climate Changes, *Curr. Clim. Chang. Reports*, 2, 148–158, <https://doi.org/10.1007/s40641-016-0049-3>, 2016.
- Westerhold, T., Röhl, U., Donner, B., McCarren, H. K., and Zachos, J. C.: A complete high-resolution Paleocene benthic stable isotope record for the central Pacific (ODP Site 1209), *Global Biogeochem. Cycles*, 25, 1–13, <https://doi.org/10.1029/2011WR010620>, 2011.
- Zachos, J., Pagani, M., Sloan, L., Thomas, E., and Billups, K.: Trends, rhythms, and aberrations in global climate 65 Ma to present, *Science* (80-.), 292, 686–693, <http://www.sciencemag.org/content/292/5517/686.short>, 2001.
- Zachos, J. C., McCarren, H., Murphy, B., Röhl, U., and Westerhold, T.: Tempo and scale of late Paleocene and early Eocene carbon isotope cycles: Implications for the origin of hyperthermals, *Earth Planet. Sci. Lett.*, 299, 242–249, <https://doi.org/10.1016/j.epsl.2010.09.004>, <http://dx.doi.org/10.1016/j.epsl.2010.09.004>, 2010.

- Zeebe, R. E.: LOSCAR: Long-term Ocean-atmosphere-Sediment Carbon cycle Reservoir model v2.0.4, *Geosci. Model Dev.*, 5, 149–166, <https://doi.org/10.5194/gmd-5-149-2012>, 2012.
- Zeebe, R. E., Westerhold, T., Littler, K., and Zachos, J. C.: Orbital forcing of the Paleocene and Eocene carbon cycle, *Paleoceanography*, 32, 440–465, <https://doi.org/10.1002/2016PA003054>, 2017.
- 5 Zhang, Y. G., Pagani, M., Liu, Z., Bohaty, S. M., and DeConto, R.: A 40-million-year history of atmospheric CO₂, *Philos. Trans. R. Soc. A Math. Phys. Eng. Sci.*, 371, <https://doi.org/10.1098/rsta.2013.0096>, <http://rsta.royalsocietypublishing.org/cgi/doi/10.1098/rsta.2013.0096>, 2013.

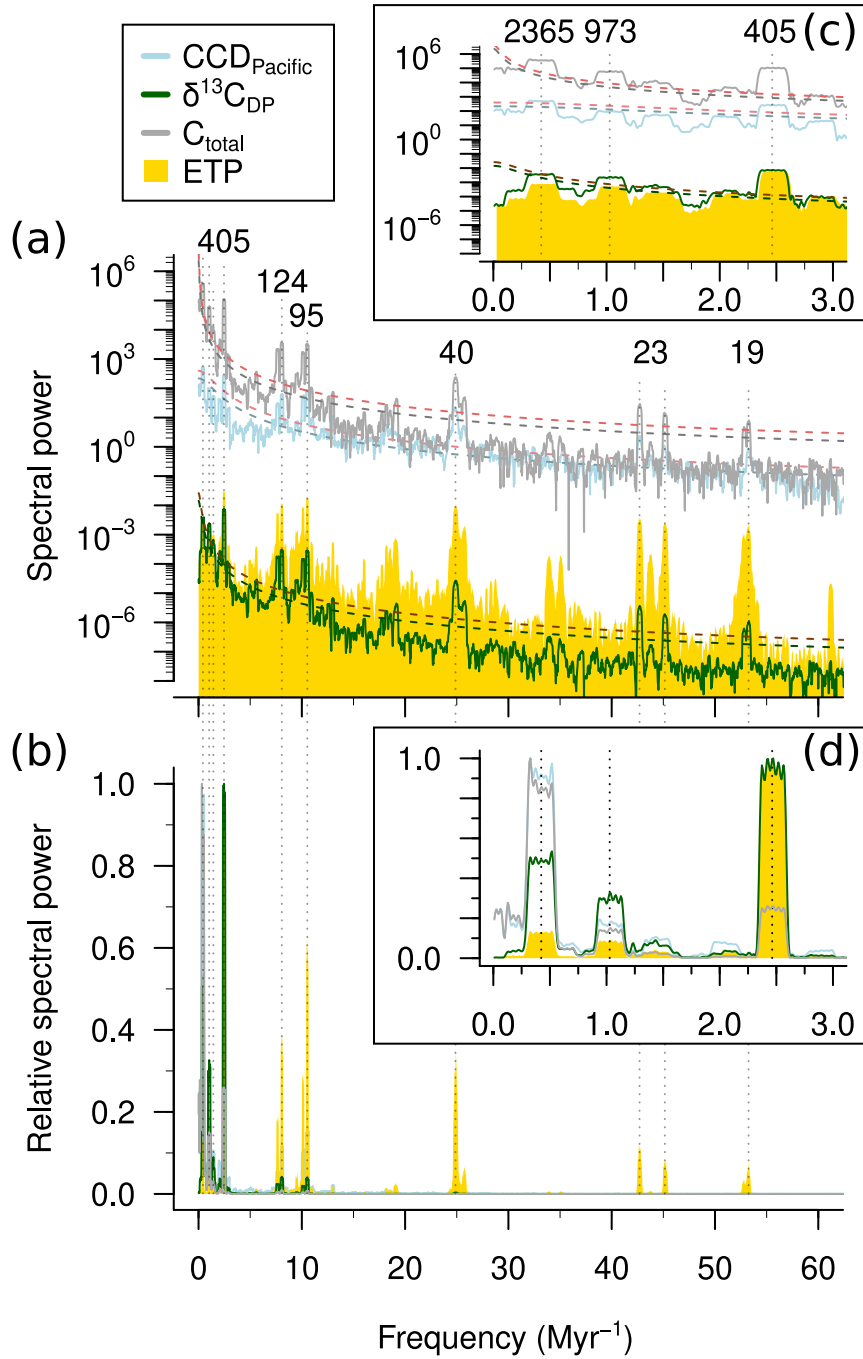


Figure 3. MTM spectral analysis of LOSCAR model output with orbital forcing strength $\alpha = 0.5$ and noise level 0.2. Shown are the model tracers and the ETP forcing used on absolute (a) (log axis) and normalized (b) (linear axis) spectral power. Relative spectral power was calculated by dividing each value by their maximum value. Insets (c) and (d) are the same as (a) and (b), but zoomed in on the frequency axis. Periods of interest (kyr^{-1}) are labelled and indicated with dashed lines.

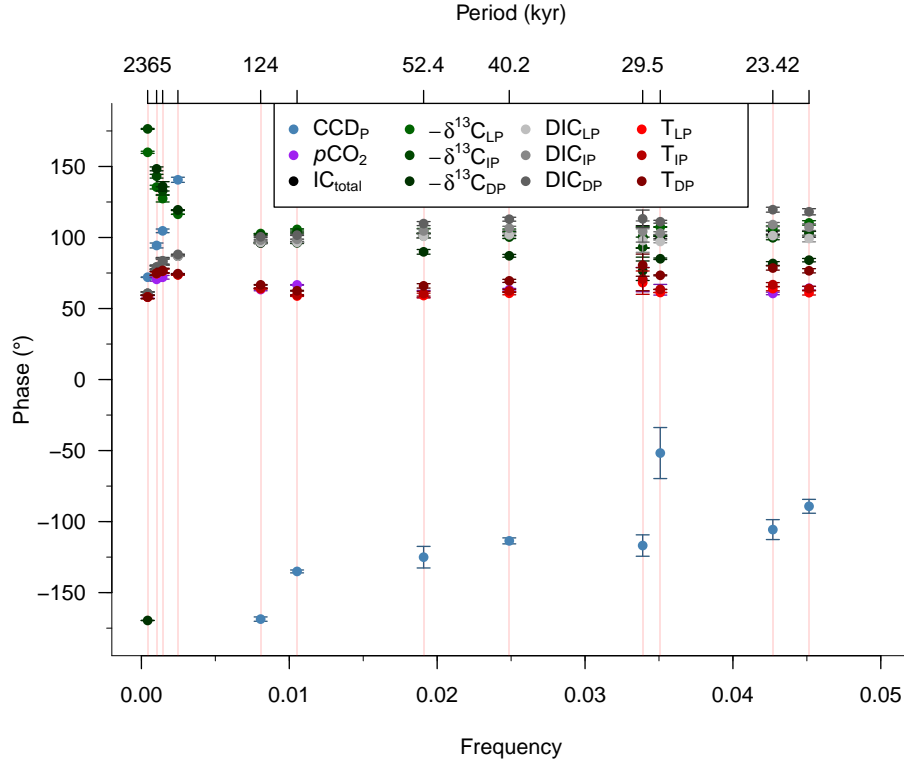


Figure 4. Phase lag ($^{\circ}$, y-axis) of the various modelled carbon cycle tracers (see legend, L stands for low-latitude surface, I for intermediate, and D for deep ocean box of the Pacific (P)) with respect to the ETP forcing (of strength 0.5 and noise 0.2) as a function of frequency (cycles/kyr, bottom x-axis) and period (kyr, top x-axis). Note minor break in x-axes to better show the low-frequency range. Error bars represent 2σ of the variation of the phase over the specified frequency intervals (red shaded regions). Note that $-\delta^{13}\text{C}$ is shown, such that a phase-lag (positive values) represents a lag of $\delta^{13}\text{C}$ -minima with respect to ETP-maxima.

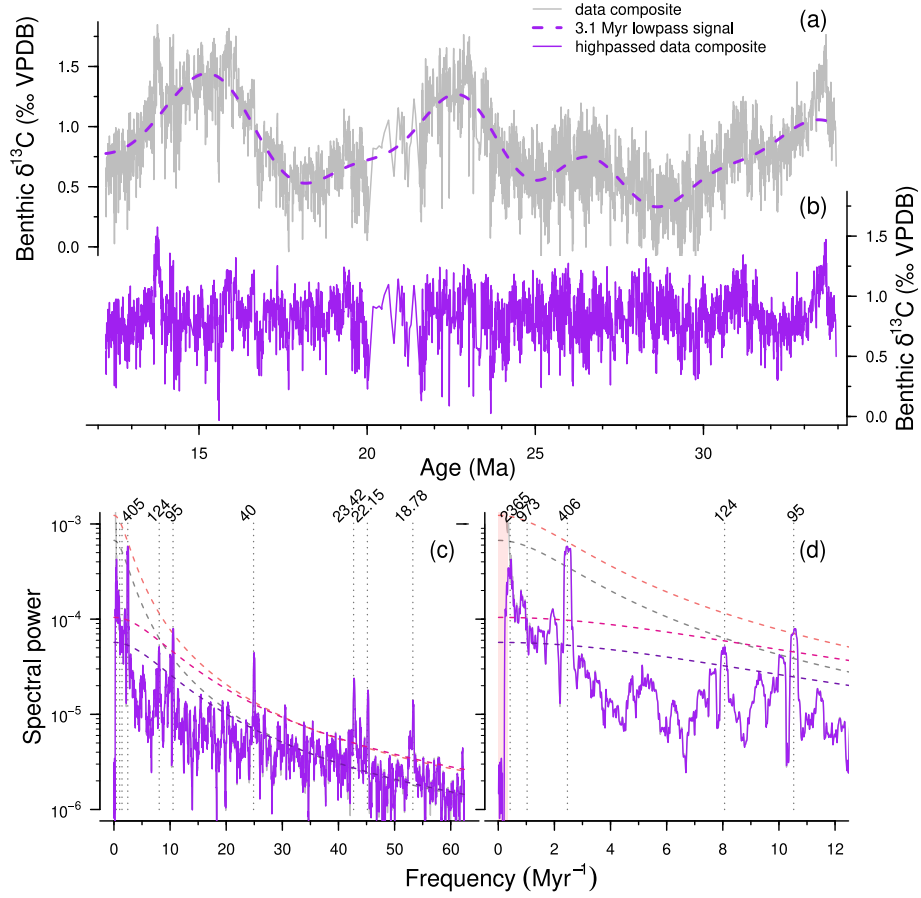


Figure 5. (a) $\delta^{13}\text{C}$ composite record (grey line) with a low-pass filter for frequencies below 3.1 Myr (dashed purple line). (b) The adjusted composite (purple) in the time domain. (c) The same records in the frequency domain. Dashed smooth lines represent the AR-1 fits for the $\delta^{13}\text{C}$ and detrended $\delta^{13}\text{C}$ records (grey and purple respectively) with associated 95 % confidence intervals (light and dark red respectively). Main orbital periods (kyr) are labelled and marked with dotted lines. (d) A zoomed-in version of (c) on the frequency axis, with the red shaded region indicating the range of the low-pass filter.

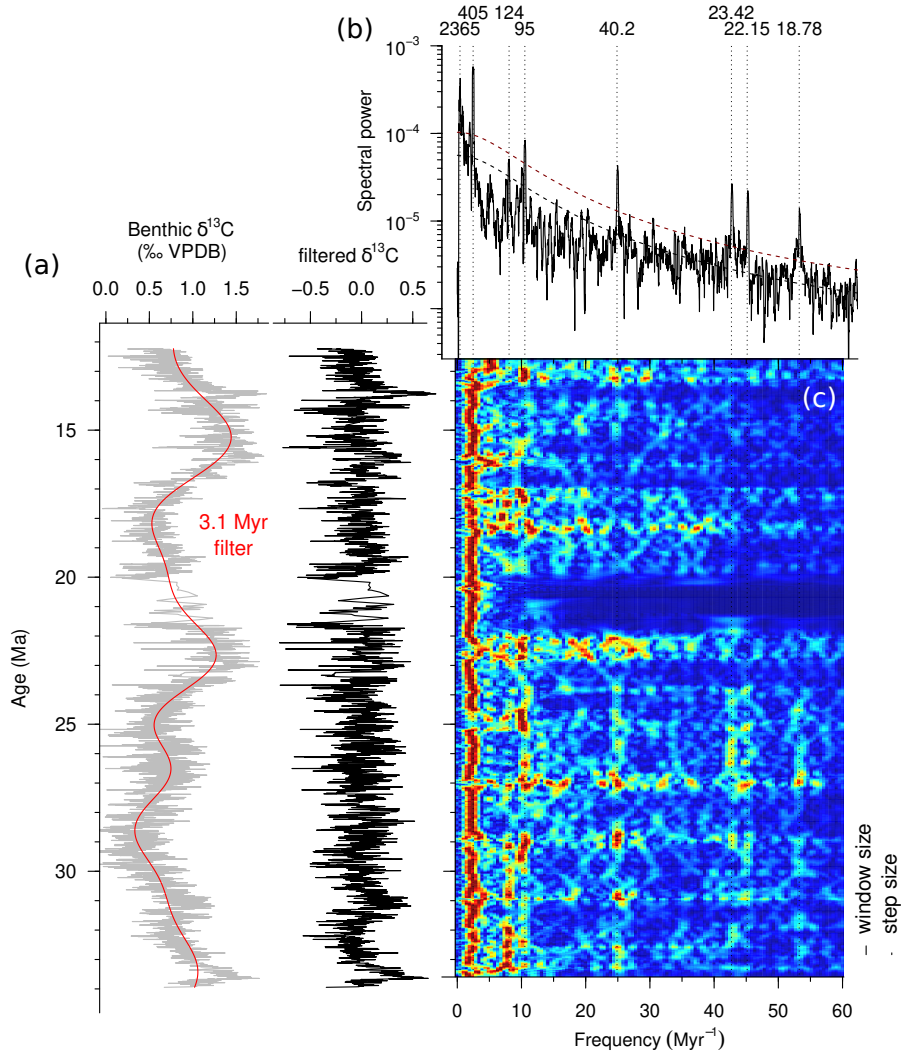


Figure 6. Evolutive multitaper harmonics analysis (c) of the data composite $\delta^{13}\text{C}$ (grey) after detrending (black) the <1 Myr signal (red line) in the time (a), frequency (b) domain. Periods of interest are labelled (b) at the same axis as (c). A window size of 0.7 Myr was used, with a step size of 10 kyr (lines on the right side in (c)). ~~Lines were added every 2.4 Myr (black horizontal lines) to be able to estimate amplitude modulation.~~ Methods adapted from Pálike et al. (2006).

Digital Supplement to ‘The 405 kyr and 2.4 Myr eccentricity components in Cenozoic carbon isotope records’

Ilja J. Kocken¹, Margot J. Cramwinckel¹, Richard E. Zeebe², Jack J. Middelburg¹, and Appy Sluijs¹

¹Department of Earth Sciences, Faculty of Geosciences, Utrecht University, Heidelberglaan 2, 3584 CS, Utrecht, The Netherlands

²Department of Oceanography, University of Hawai‘i at Mānoa, 1000 Pope Road, HI 96822, Honolulu, USA

Correspondence: Ilja J. Kocken (i.j.kocken@uu.nl)

1 Calcite compensation depth outliers

The large number of very low values in the CCD can be explained by the steady state alternating between two or more sediment boxes. This could also be the cause of the relatively stronger precession and obliquity peaks in the CCD’s spectrum (Fig. ?? (c)), wherein the large high-frequency perturbations overshadow the long-term trend. The identical spectral outcome of a medium noise-only run (supplement fig. 4) further substantiates this assessment. These issues could be resolved by increasing the limitation: the finite number of sediment boxes in the model to generate a smoother CCD curve.

2 Calcite compensation depth spectral analysis

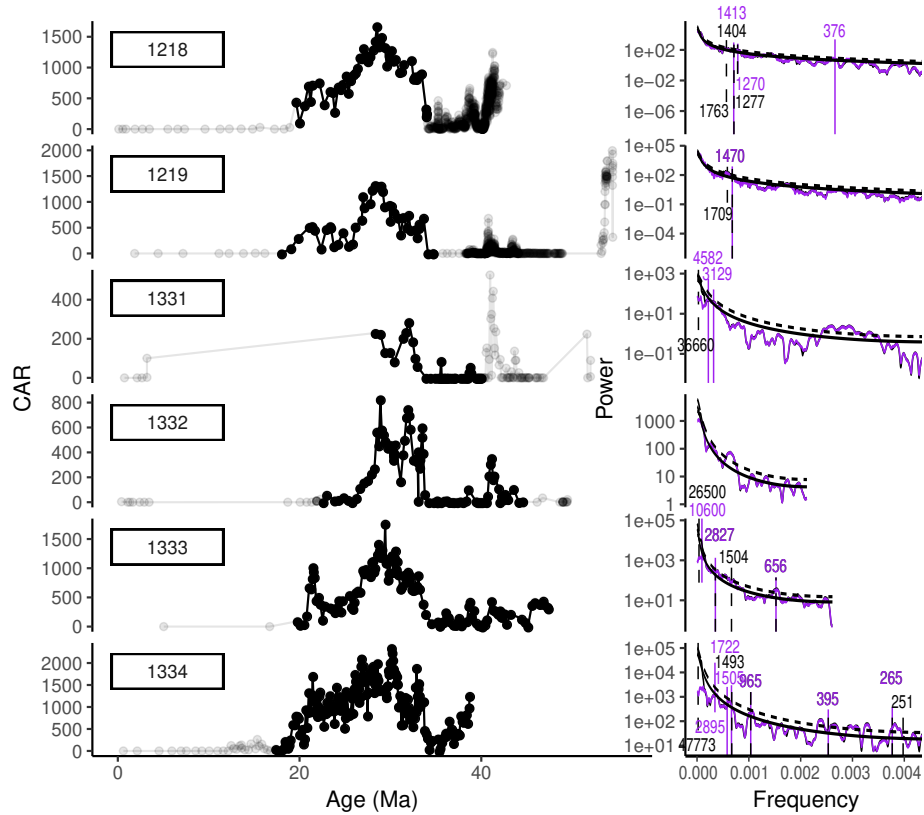


Figure 1. Carbonate accumulation rate (CAR) in the time (left side) and frequency domains (right side) for all sites in Pälke et al. (2012). Loess filtered (purple) and unfiltered (black) MTM-spectra are shown (right side) for the selected time-slices (darker dots in left side). Time-slices were selected based on continuous similar-resolution intervals where there are no known time-scale issues. Corresponding significant (harmonic f-test) peaks are labelled with associated periods.

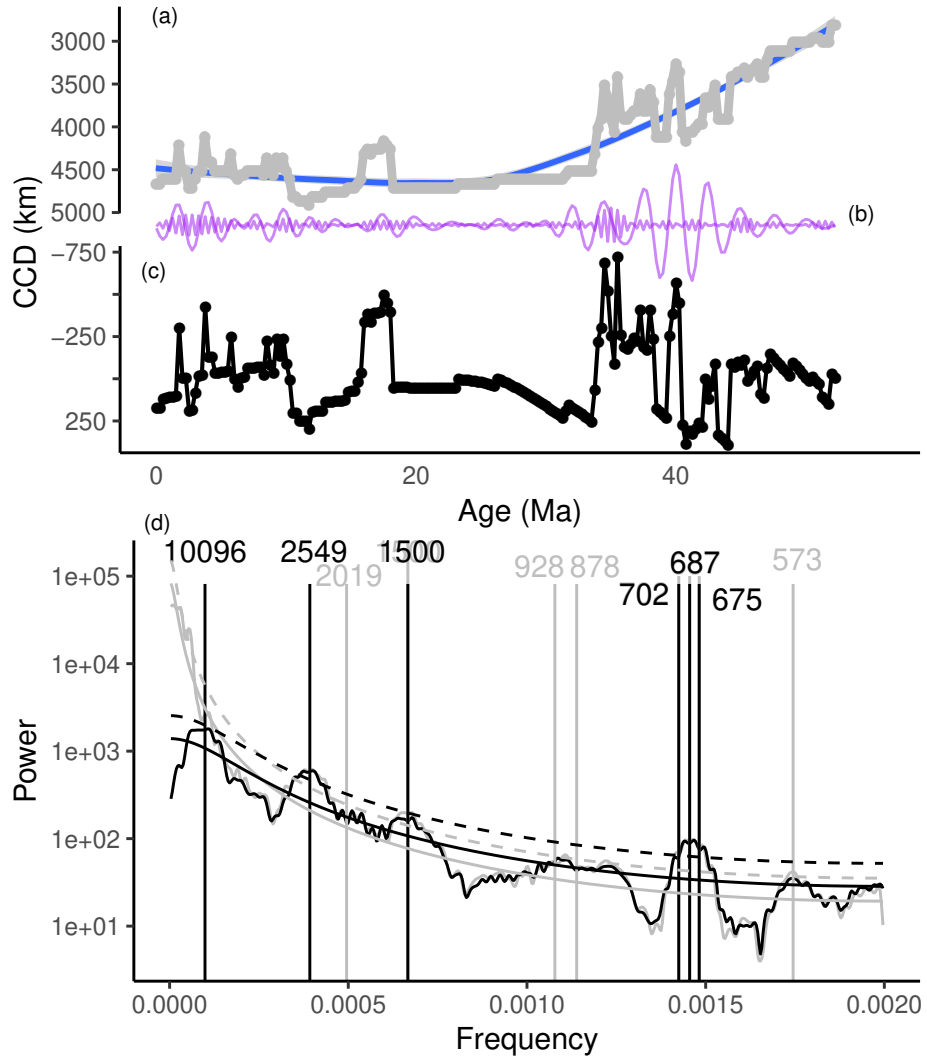


Figure 2. CCD as reconstructed by Pálke et al. (2012) (a), filtered for 405 kyr and 2.4 Myr (b) with a loess fit (a, blue line) subtracted from the record (c), which result in power spectra for the original (gray) and detrended (black) Pacific CCD composite (c). Significant peaks are labelled with the corresponding periods.

Table 1. Periods of interest in the input forcing were calculated from dominant secular frequencies (g , from Laskar et al. (2004)). Non-eccentricity typical periods were found visually with by analysing in detail the MTM-spectra of component. The index i in g_i refers to the planet in the solar system (counting from the sun outward).

Component	Terms	Period (yr)	Plot period (kyr)
Eccentricity	$g_4 - g_3$	2365408.22085889	2365
Eccentricity	$g_1 - g_5$	972584.643914338	973
Eccentricity	$g_2 - g_1$	696021.261160021	696
Eccentricity	$g_2 - g_5$	405691.71449262	405
Eccentricity	$g_2 - g_4$	123854.477912872	124
Eccentricity	$g_4 - g_5$	94886.4059134611	95
Obliquity			52.4
Obliquity			40.2
Obliquity			29.5
Obliquity			28.5
Precession			23.42
Precession			22.15
Precession			18.78
Precession			16.34

3 Effects of shifting records for consistency in overlap

Attempts were made to improve inter-record compatibility by shifting record $\delta^{13}\text{C}$ and $\delta^{18}\text{O}$ values from the various studies towards heavier or lighter values, such that mean isotope values in overlapping regions would be identical, but were eventually abandoned because of their minor influence on spectral outcome (~~supplement~~Supp. Fig. 3).

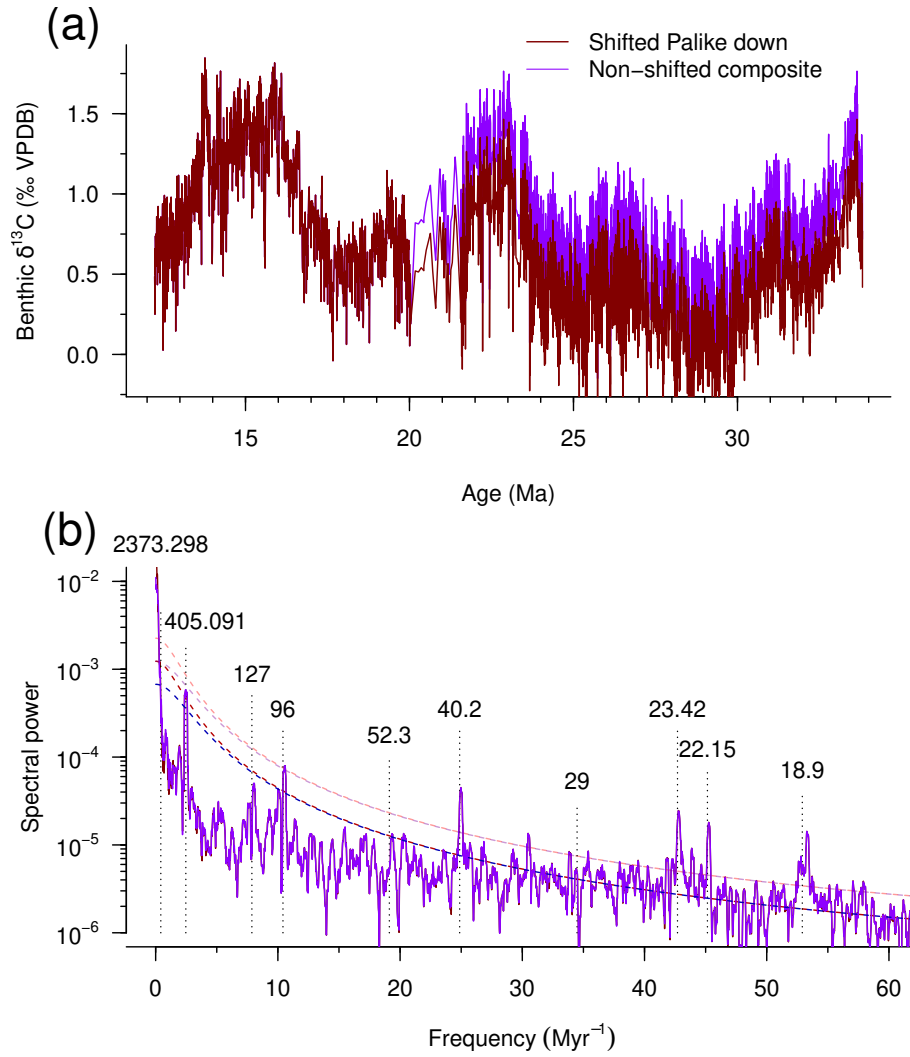


Figure 3. A linear shift in the record by Pálike et al. (2006) (down by 0.30‰ VPDB in red, original in blue) increases consistency between records in the area of overlap (where data from Pálike et al. (2006) were omitted due to lower resolution) but hardly effects spectral outcome and is therefore not used in this study.

Table 2. Effects of increasing various parameters on model output.

Increased parameter	Causes this effect
initial pCO ₂	Base level of $\delta^{13}\text{C}$ increases
orbstrength	Amplitude of cycle variation in tracers increases
cliplevel	Increased shift in spectral power to lower frequencies
E, T and P in ETP	Shift spectral power to associated frequencies
noiselevel	Amplitude of noise increases, base of AR-1 fit in MTM-spectra is raised
noisetiming	More noise is generated in lower frequency range

4 Model sensitivity

The introduction of white noise on C_{org} burial results in red noise in the spectral output of the model tracers. This basically means that the low-frequency spectral power amplification that we see in the orbitally-forced runs also occurs for the noise input. The addition of noise thus adds spectral power to the low-frequency range, and raises the background levels of MTM-
5 spectra in the orbitally-forced model output tracers.

The model responds as expected to changes in initial conditions and newly added parameters. Table 2 shows an overview of what happens to the model output when a parameter is increased.

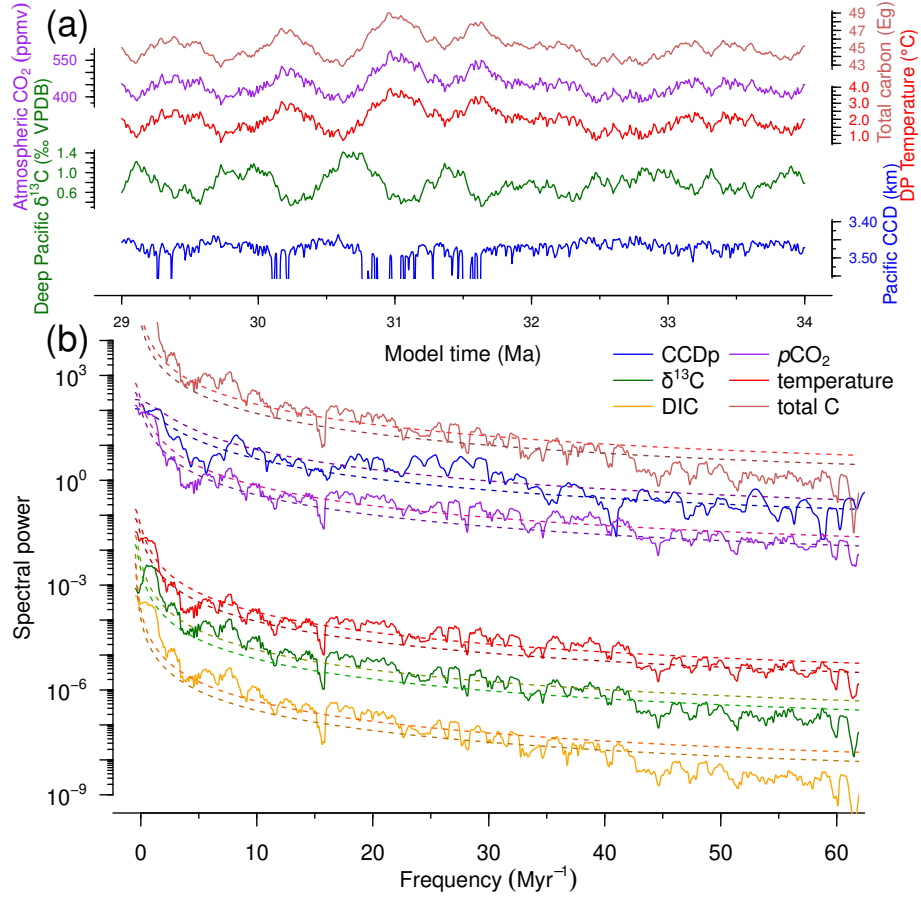


Figure 4. Model output when $\text{C}_{\text{org}}\text{-C}_{\text{org}}$ burial is only affected by noise that is generated every time a time step larger than 1 kyr has passed in the time (A) and frequency (B) domain.

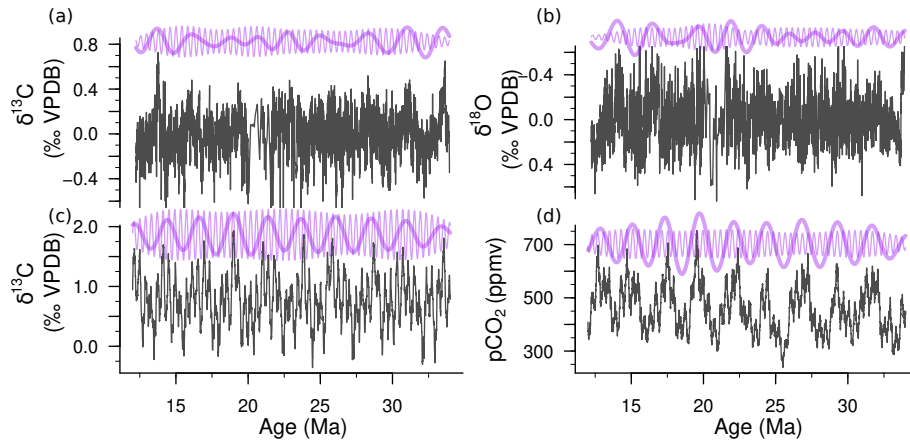


Figure 5. A run without noise, where 490 W m^{-2} clipped 65°N summer insolation is used. Comparison of the detrended data composite of $\delta^{13}\text{C}$ (a) and $\delta^{18}\text{O}$ (b) to model output $\delta^{13}\text{C}$ (c) and $p\text{CO}_2$ (d) forced with ETP (1:0.5:−0.4) with an orbital forcing of 0.5 and noise level of 0.2. 2.4 Myr and 405 kyr bandpass filters are shown in purple (shifted up by arbitrary amount).

5 Apparent lead in 2.4 Myr of the $-\delta^{13}\text{C}_{\text{DP}}$ signal

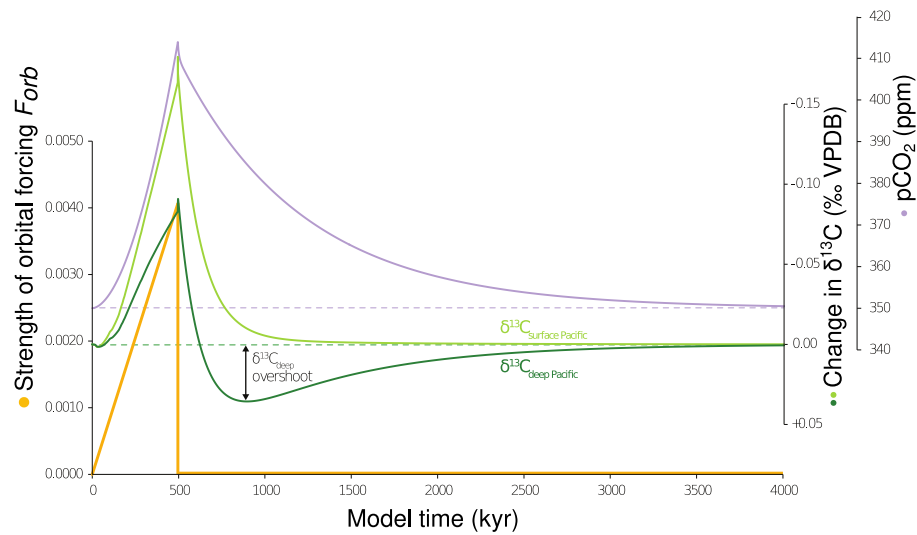


Figure 6. Transient linearly increasing orbital forcing (orange line) and the response of $\delta^{13}\text{C}$ (green line) and pCO_2 (purple line). Horizontal dotted lines are visual aids to track the initial values of $\delta^{13}\text{C}$ and pCO_2 . The double arrow marked “ $\delta^{13}\text{C}$ overshoot” is drawn between the initial value of $\delta^{13}\text{C}$ and the maximum value reached after cessation of forcing.

The $\delta^{13}\text{C}$ of DIC in deep and intermediate ocean boxes shows a lead to the 2.4 Myr eccentricity forcing. A close assessment of the first few peaks in the 2.4 Myr bandpass filtered deep-ocean $\delta^{13}\text{C}$ reveals that the lead only appears from the second peak onward, indicating that it may be an overshoot in the carbon isotope response to the forcing. Simulations with a transient, linearly increasing forcing were performed to explore whether the proposed overshoot could be found (Fig. 6). In this simulation, the imposed forcing decreased net burial of C_{org} for 500 kyr. During this time, pCO_2 progressively increases while $\delta^{13}\text{C}$ of DIC becomes more depleted. After the forcing has been terminated at $t = 500$ kyr, pCO_2 slowly decreases to its initial value over millions of years by the feedback of continental weathering. In contrast, carbon isotopes return to their initial value much more rapidly and subsequently overshoot past it. A maximum $\delta^{13}\text{C}$ value is reached at $t = 895$ kyr, almost 400 kyr after the forcing has stopped. This confirms that the observed lead of carbon isotopes to the 2.4 Myr eccentricity cycle is an overshoot response rather than an actual lead. Additionally, the slow development of the overshoot explains why it does not result in a lead to the shorter 405 and 100 kyr cycles. The remaining question is why the overshoot develops in deep and intermediate ocean $\delta^{13}\text{C}$, but not in the surface ocean (Fig. ?? and Fig. 6). At any time, the mean $\delta^{13}\text{C}$ value of an ocean box represents a balance between the magnitude of carbon fluxes going in and out of the box and their isotopic signature. The LOSCAR model shows similar results as the box model runs by Kump (1991), which reveal that at steady state, surface ocean $\delta^{13}\text{C}$ follows the following equation:

$$\delta^{13}\text{C}_{\text{surface}} = \delta^{13}\text{C}_{\text{weathering}} - \Delta^{\text{photo}} \times (F_{\text{burial}}^{\text{OC}} / [F_{\text{burial}}^{\text{OC}} + F_{\text{burial}}^{\text{IC}}]) \quad (1)$$

Surface ocean $\delta^{13}\text{C}$ thus depends on three factors: the ratio between burial rates of organic ($F_{\text{burial}}^{\text{OC}}$) and inorganic carbon ($F_{\text{burial}}^{\text{IC}}$), the $\delta^{13}\text{C}$ of weathered carbon ($\delta^{13}\text{C}_{\text{weathering}}$), and the magnitude of isotopic fractionation during photosynthesis (Δ^{photo}). As $\delta^{13}\text{C}$ weathering and Δ^{photo} are constant parameters in the model, $\delta^{13}\text{C}$ surface becomes lighter when relatively less organic carbon is buried, and vice versa. The carbon isotopic gradient between surface and deep ocean $\delta^{13}\text{C}$ can then be calculated according to the following equation (Broecker and Peng, 1982; Tyrrell and Zeebe, 2004):

$$\Delta\delta^{13}\text{C} = -\Delta^{\text{photo}} \times \Delta[\text{DIC}] / [\text{DIC}]_{\text{mean}} \quad (2)$$

While $\delta^{13}\text{C}_{\text{surface}}$ is independent of internal oceanic processes, $\delta^{13}\text{C}_{\text{deep}}$ is determined by Δ^{photo} and the ratio between deep and surface DIC ($\Delta[\text{DIC}]$) compared to the mean DIC of the ocean ($[\text{DIC}]_{\text{mean}}$). As $\Delta[\text{DIC}]$ is dominantly controlled by the organic carbon pump, this can be interpreted as maintenance of the surface-to-deep isotope gradient by the biological pump.

Since both Δ^{photo} and the strength of the biological pump are constant in the model, changes in the gradient are mainly caused by the size of the total oceanic carbon inventory, reflected by $[\text{DIC}]_{\text{mean}}$. During the first 500 kyr of the simulation, both $\delta^{13}\text{C}$ surface and $\delta^{13}\text{C}$ deep become more ^{13}C -depleted as C_{org} burial is decreasing relative to IC burial. After the forcing has terminated, C_{org} burial instantaneously increases back to initial conditions. However, $[\text{DIC}]_{\text{mean}}$ and pCO_2 are still enhanced relative to the initial conditions for several Myr, thereby elevating both silicate and carbonate weathering (equations 1 and 2). During this rebound phase, $\delta^{13}\text{C}$ surface slowly increases back to its initial value, as burial of IC is enhanced relative to C_{org} burial. In addition to this, the elevated inventory of oceanic carbon diminishes the isotope gradient by decreasing

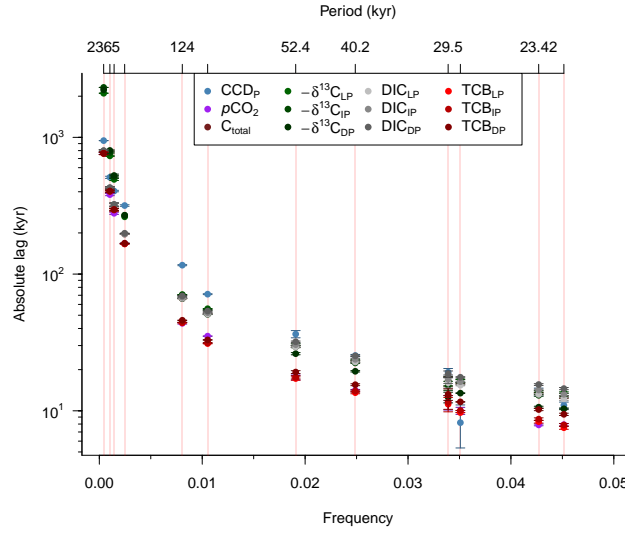


Figure 7. Absolute phasing (lags and leads indistinguishable) in absolute ages (kyr, log axis) as a function of frequency (cycles/kyr).

$\Delta[\text{DIC}]/[\text{DIC}]_{\text{mean}}$ (the small increase in $\Delta[\text{DIC}]$ is negligible compared to that in $[\text{DIC}]_{\text{mean}}$). This can be interpreted as a relative decrease in strength of the organic carbon pump compared to the size of the total carbon inventory, causing the deep isotopes to increase even more than those of the surface and resulting in the observed overshoot of $\delta^{13}\text{C}_{\text{DP}}$.

6 2.4 Myr amplitude modulation of the shorter eccentricity cycles

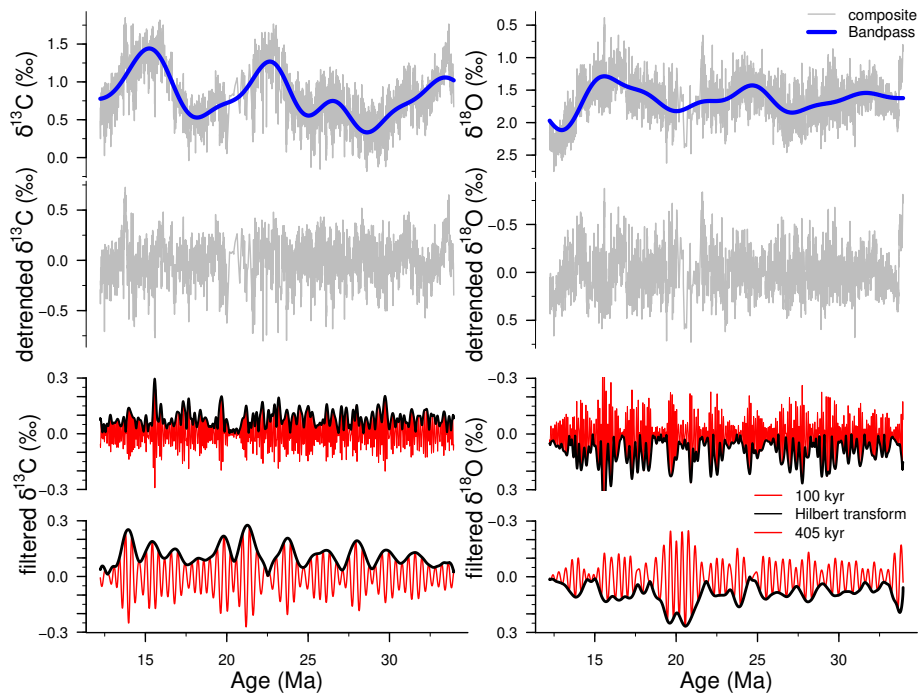


Figure 8. The envelopes (black) of the 100 and 405 kyr filtered (red) composite record (gray) show a clear 2.4 Myr cycle in $\delta^{13}\text{C}$ (~~(a~~left side~~)~~
~~;~~~~(e))~~, which is even more pronounced in the ~~and~~ $\delta^{18}\text{O}$ (~~(b~~right side~~)~~~~;~~~~(e))~~). This is additional evidence for 2.4 Myr amplitude modulation of the 100 and 405 kyr eccentricity cycles.

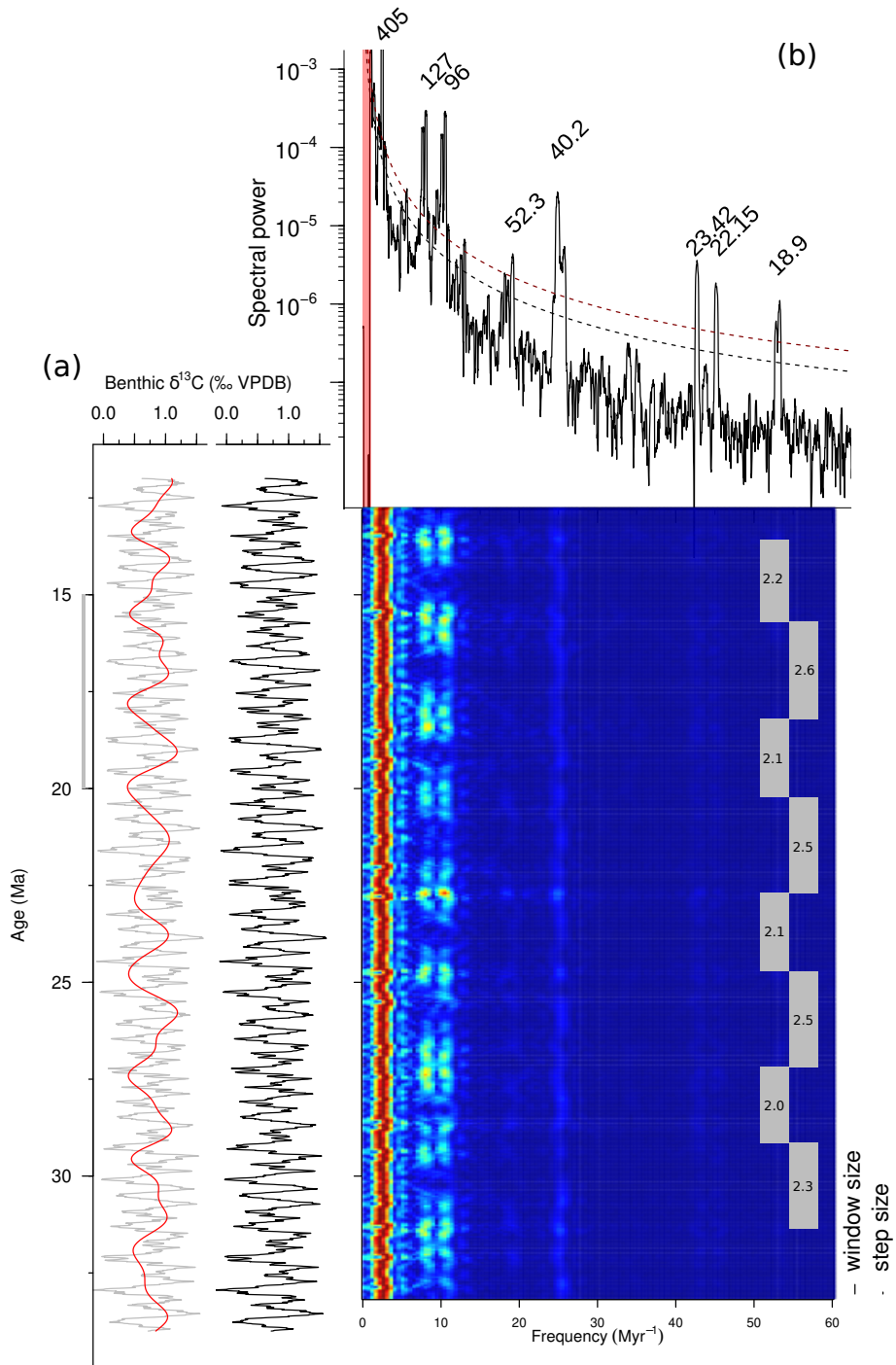


Figure 9. ~~EHA-analysis~~ Evolutive multitaper harmonics analysis (c) of the ~~detrended data composite~~ model output $\delta^{13}\text{C}$ (grey) after detrending (black) the <1 Myr signal (red line) in the time (a), ~~ETP-frequency (0.7:1.25:2.7b)~~ domain. Periods of interest are labelled (b) at the same axis as (c). Distances between peaks in the 100 kyr period of short eccentricity are marked (gray boxes with duration). A window size of 0.7 Myr was used, ~~detrended model~~ $\delta^{13}\text{C}$ when forced with a step size of 10 kyr (lines on the ~~clipped insolation and noise~~ right side in (c) and 65°N summer insolation clipped at 490 W m^{-2} (14. See main-text FigMethods adapted from Pálke et al. (2006). ?? for explanation.

References

- Broecker, W. and Peng, T.-H.: Tracers in the sea, Lamont-Doherty Geological Observatory, Columbia University, 1982.
- Kump, L. R.: Interpreting carbon isotope excursions: Strangelove oceans, *Geology*, 19, 299–302, [https://doi.org/10.1130/0091-7613\(1991\)019<0299, 1991](https://doi.org/10.1130/0091-7613(1991)019<0299, 1991).
- 5 Laskar, J., Robutel, P., Joutel, F., Gastineau, M., Correia, a. C. M., and Levrard, B.: Astrophysics A long-term numerical solution for the insolation, *Astronomy*, 285, 261–285, <https://doi.org/10.1051/0004-6361>, <http://www.edpsciences.org/10.1051/0004-6361:20041335>, 2004.
- Pälike, H., Norris, R. D., Herrle, J. O., Wilson, P. A., Coxall, H. K., Lear, C. H., Shackleton, N. J., Tripathi, A. K., and Wade, B. S.: The heartbeat of the Oligocene climate system., *Science*, 314, 1894–8, <https://doi.org/10.1126/science.1133822>, <http://www.sciencemag.org/content/314/5807/1894.abstract>{ % }5Cn<http://www.sciencemag.org/content/314/5807/1894>, 2006.
- 10 Pälike, H., Lyle, M. W., Nishi, H., Raffi, I., Ridgwell, A., Gamage, K., Klaus, A., Acton, G., Anderson, L., Backman, J., Baldauf, J., Beltran, C., Bohaty, S. M., Bown, P., Busch, W., Channell, J. E., Chun, C. O., Delaney, M., Dewangan, P., Dunkley Jones, T., Edgar, K. M., Evans, H., Fitch, P., Foster, G. L., Gussone, N., Hasegawa, H., Hathorne, E. C., Hayashi, H., Herrle, J. O., Holbourn, A., Hovan, S., Hyeong, K., Iijima, K., Ito, T., Kamikuri, S. I., Kimoto, K., Kuroda, J., Leon-Rodriguez, L., Malinverno, A., Moore, T. C., Murphy, B. H., Murphy,
- 15 D. P., Nakamura, H., Ogane, K., Ohneiser, C., Richter, C., Robinson, R., Rohling, E. J., Romero, O., Sawada, K., Scher, H., Schneider, L., Sluijs, A., Takata, H., Tian, J., Tsujimoto, A., Wade, B. S., Westerhold, T., Wilkens, R., Williams, T., Wilson, P. A., Yamamoto, Y., Yamamoto, S., Yamazaki, T., and Zeebe, R. E.: A Cenozoic record of the equatorial Pacific carbonate compensation depth, *Nature*, 488, 609–614, <https://doi.org/10.1038/nature11360>, <http://dx.doi.org/10.1038/nature11360>, 2012.
- Tyrrell, T. and Zeebe, R. E.: History of carbonate ion concentration over the last 100 million years, *Geochim. Cosmochim. Acta*, 68, 3521–
- 20 3530, <https://doi.org/10.1016/j.gca.2004.02.018>, 2004.

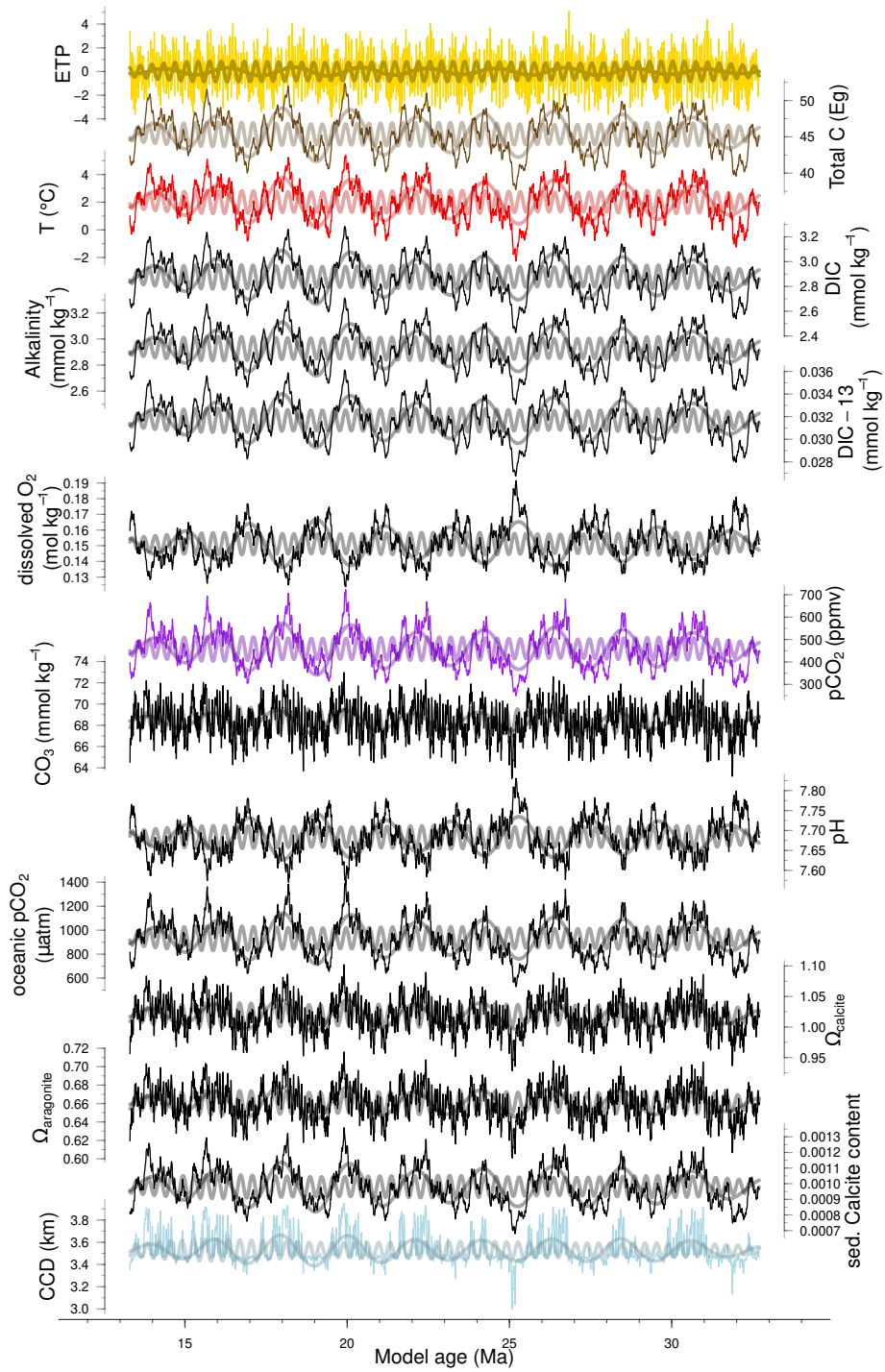


Figure 10. Example time-series model output for an ETP-forced (1:0.5:-0.4) run with `orbstrength` 0.5 and `noiselevel` 0, showing all model output tracers, except PO_4 , because it is constant throughout at $2.62 \mu\text{mol kg}^{-1}$. 405 kyr (frequency of $2.46 \pm 0.15 \text{ Myr}^{-1}$) and 2.4 Myr ($0.42 \pm 0.15 \text{ Myr}^{-1}$) bandpass filters are shown for all records (thick darker lines).

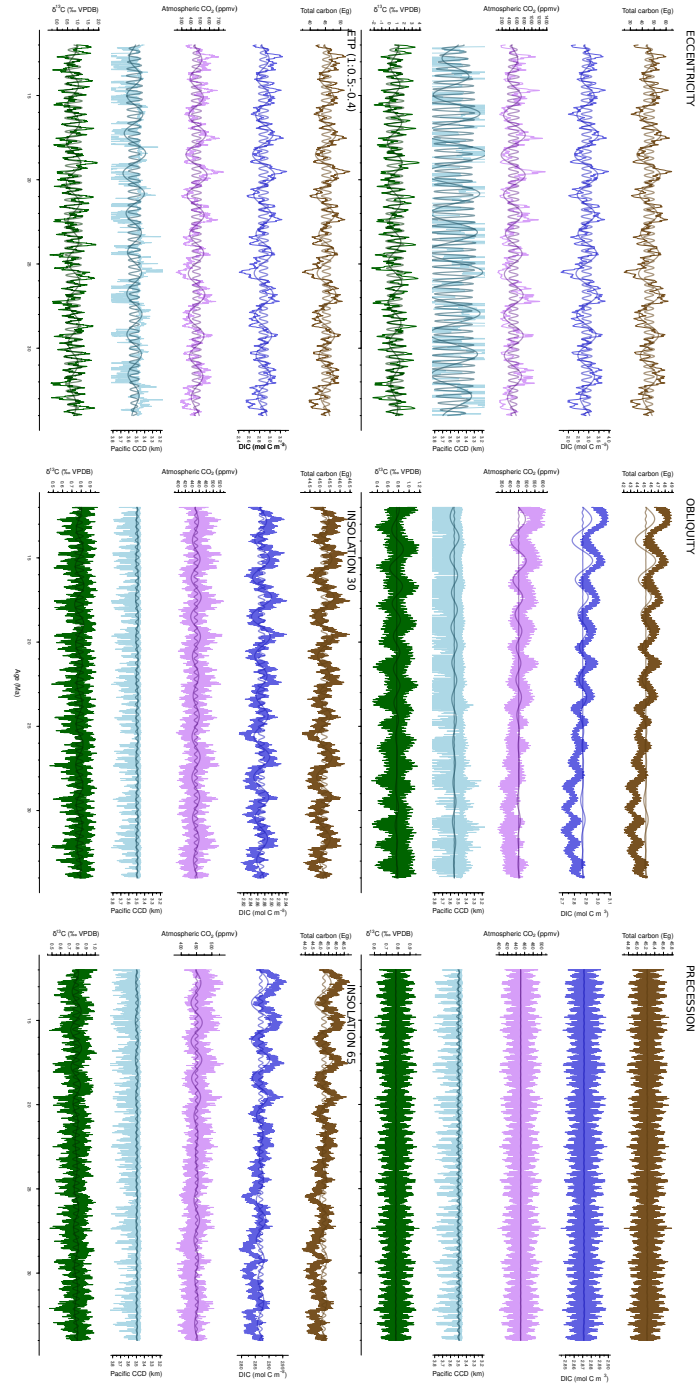


Figure 11. Time series model output with eccentricity, obliquity, precession, ETP (1:0.5:-0.4), 30°N and 65°N insolation forcing. Thick lines through the tracers represent 405 kyr and 2.4 Myr filters.